

CNWRA *A center of excellence in earth sciences and engineering*

A Division of Southwest Research Institute™
6220 Culebra Road • San Antonio, Texas, U.S.A. 78228-5166
(210) 522-5160 • Fax (210) 522-5155

June 22, 2000
Contract No. NRC-02-97-009
Account No. 20.01402.671

U.S. Nuclear Regulatory Commission
ATTN: Dr. Mysore S. Nataraja
Division of Waste Management
TWFN (Mail Stop 7-C6)
Washington, DC 20555

Subject: Repository Design and Thermal-Mechanical Effects Key Technical Issue Intermediate Milestone No. 20.01402.671.040, Thermal-Mechanical Effect on Repository Design/Performance: Continuum Model—Conference Paper or Journal Article

Dear Dr. Nataraja:

Attached is the Center for Nuclear Waste Regulatory Analyses (CNWRA) document entitled “Thermal-Mechanical Effects on Long-Term Hydrological Properties at the Proposed Yucca Mountain Nuclear Waste Repository.” In accordance to my verbal agreement with you, this deliverable is being submitted as a CNWRA report instead of a conference paper or journal article that was originally identified in the Operations Plan. This technical document fulfills the requirements for the subject milestone which is due June 23, 2000.

An estimation of the change in hydrological properties due to thermal-mechanical (TM) effects at the proposed Yucca Mountain repository is important because of potential effects on the percolation flux through the repository horizon, which could have significant effects on water influx into emplacement drifts, waste-package corrosion, and waste mobilization and transport to the underlying water table. TM effects on hydrological properties is a component of Subissue 3 of the RDTME KTI. This report reviews the technical bases for the DOE position that states “thermal loading will produce negligible changes in rock hydraulic properties” and presents results from alternative model calculations of TM effects on hydrological properties. The alternative model calculations indicate that TM induced permeability increase may be greater than the upperbound suggested by the DOE. Furthermore, lateral flow of moisture within the zones affected by such hydrological-property change can be expected and would result in elevated water flux impacting emplacement-drift sections within the affected zone.

If you have any questions on this report, please contact me at (210) 522-5151 or Goodluck Ofoegbu at (210) 522-6641.

Sincerely yours,



Asadul H. Chowdhury, Manager
Mining, Geotechnical, and
Facility Engineering



Washington Office • Twinbrook Metro Plaza #210
12300 Twinbrook Parkway • Rockville, Maryland 20852-1606

ACH/cp

d:\support\asad\letters\1402671040.wpd

cc: J.Greeves N. Stablein P. Justus S. Hsiung
J. Holonich D. Brooks B. Leslie A. Ghosh
W. Reamer D. Galvin J. Pohle R. Chen
D. DeMarco B. Jagannath W. Patrick D. Gute
B. Meehan T. Ahn CNWRA Directors G. Ofoegbu
J. Linehan D. Dancer CNWRA Element Managers B. Dasgupta
(w/o enclosure) T. McCartin P. Maldonado (SwRI Contracts) D. Hughson
R. Green

**THERMAL-MECHANICAL EFFECTS ON LONG-TERM
HYDROLOGICAL PROPERTIES AT THE PROPOSED
YUCCA MOUNTAIN NUCLEAR WASTE REPOSITORY**

Prepared for

**Nuclear Regulatory Commission
Contract NRC-02-97-009**

Prepared by

**Center for Nuclear Waste Regulatory Analyses
San Antonio, Texas**

June 2000



**THERMAL-MECHANICAL EFFECTS ON LONG-TERM
HYDROLOGICAL PROPERTIES AT THE PROPOSED
YUCCA MOUNTAIN NUCLEAR WASTE REPOSITORY**

Prepared for

**Nuclear Regulatory Commission
Contract NRC-02-97-009**

Prepared by

Goodluck Ofoegbu

**Center for Nuclear Waste Regulatory Analyses
San Antonio, Texas**

June 2000

ABSTRACT

Geomechanical response to thermal loading at the proposed Yucca Mountain repository for high-level nuclear waste may result in changes in rock-mass hydrological properties. A change in hydrological properties is important because of potential effects on the percolation flux through the repository horizon, which has significant effects on water influx into emplacement drifts, waste-package corrosion, and waste mobilization and transport to the underlying water table. Results from numerical modeling are presented to argue that significant thermally induced changes in hydrological properties can be expected and would result in a redistribution of percolation flux at the repository horizon. The results lead to the following conclusions: (i) rock-mass permeabilities near the repository horizon can be expected to increase within laterally discontinuous zones centered at the emplacement drifts and in the middle of interdrift pillars, owing to fracture dilation associated with geomechanical response to thermal loading; (ii) the magnitude of permeability increase would be greater around the drift openings than in the pillars, and would depend on thermal loading, rock-mass mechanical properties, and time-dependent mechanical degradation; (iii) altered zones characterized by horizontal-fracture dilation in areas of high rock-mass quality and vertical-fracture dilation in areas of low rock-mass quality can be expected, but fracture closure from thermally induced stresses is likely to be small and insignificant to rock-mass permeability; and (iv) lateral flow of moisture can be expected in the altered zones and would result in elevated vertical percolation flux within and at the downstream end of the altered zones. Therefore, parts of an emplacement drift close to the downstream end of an altered zone can be expected to experience elevated percolation flux. These findings contrast with a U.S. Department of Energy position that "thermal loading will produce negligible changes in rock hydrologic properties."

CONTENTS

Section	Page
FIGURES	vii
TABLES	ix
ACRONYMS	xi
ACKNOWLEDGMENTS	xiii
1 INTRODUCTION	1-1
1.1 BACKGROUND	1-1
1.2 U.S. DEPARTMENT OF ENERGY PREDICTIONS OF THERMAL- MECHANICAL EFFECTS ON HYDROLOGICAL PROPERTIES	1-2
2 DESCRIPTION OF MODEL	2-1
2.1 CONTINUUM MODEL FOR FRACTURE DILATION	2-1
2.2 MODEL GEOMETRY FOR THERMAL-MECHANICAL ANALYSES	2-3
2.3 BOUNDARY AND INITIAL CONDITIONS	2-3
2.4 THERMAL LOADING	2-5
2.5 THERMAL AND MECHANICAL PROPERTIES	2-5
2.5.1 Thermal Properties	2-6
2.5.2 Mechanical Properties	2-6
2.5.3 Rock-Mass Degradation from Geochemical Alteration of Fracture-Wall Rock	2-8
2.6 ANALYSIS PROCEDURE	2-9
3 ANALYSIS RESULTS	3-1
3.1 THERMAL ANALYSIS RESULTS	3-1
3.2 FRACTURE APERTURE CHANGE FROM ELASTIC ROCK-MASS RESPONSE	3-1
3.3 FRACTURE PERMEABILITY CHANGE FROM INELASTIC ROCK-MASS RESPONSE	3-6
3.3.1 Effects of Specific Heat and Thermal Expansivity	3-6
3.3.2 Effects of Rock-Mass Quality	3-8
3.3.3 Effects of Mechanical Degradation	3-8
3.3.4 Effects of Thermal Loading	3-12
4 EFFECTS OF THERMAL-MECHANICAL-ALTERED ZONES ON MOISTURE FLOW	4-1
5 CONCLUSIONS	5-1
6 REFERENCES	6-1

FIGURES

Figure	Page
2-1	Outline of model domain (solid lines) showing (a) full model and (b) part of model within 50 m above and below the drift axis 2-4
2-2	Postulated degradation curve for rock-mass cohesion, representing the effects of geochemical alteration of fracture-wall rock 2-9
3-1	Temperature distributions at 150 yr following waste emplacement for cases with (a) temperature-dependent heat capacity and (b) constant heat capacity 3-2
3-2	Variation of fracture aperture with depth below bedrock surface based on data developed by Snow (1968). 3-3
3-3	Distributions of vertical and horizontal stresses (σ_v and σ_h) at 150 yr following waste emplacement 3-5
3-4	Distributions of fracture-permeability change ratio R_k at 150 yr following waste emplacement 3-7
3-5	Effects of rock-mass quality and mechanical degradation on distributions of fracture-permeability change ratio R_k 3-9
3-6	Discontinuum model results showing the effects of rock-mass quality on distributions of fracture slip at 150 yr following waste emplacement. 3-10
3-7	Effects of rock-mass stiffness on distributions of fracture-permeability change ratio R_k associated with inelastic response in RMQ1 areas at 150 yr 3-11
3-8	Distribution of fracture-permeability change ratio R_k associated with inelastic response at 150 yr 3-13
4-1	Finite difference discretization of an east-west vertical section through Yucca Mountain for TH analyses 4-2
4-2	Profiles of percolation flux at the repository depth, illustrating the effects of a generic TM-altered zone. Results represent the effects of horizontal-fracture dilation with no change in vertical fractures 4-3
4-3	Profiles of percolation flux at the repository depth, illustrating the effects of a generic TM-altered zone. Results represent the effects of combining horizontal-fracture dilation with different magnitudes of net vertical-fracture dilation and closure 4-4

TABLES

Table		Page
2-1	Yucca Mountain geothermal gradient (Civilian Radioactive Waste Management System, Management and Operating Contractor, 1997a)	2-5
2-2	Specific heat capacity for the lower lithophysal unit of Topopah Spring Welded Tuff, described as a function of temperature	2-6
2-3	Thermal expansivity of Topopah Spring Welded Tuff described as a function of temperature	2-7
2-4	Rock-mass strength parameters obtained using empirical relationships from Hoek and Brown (1997)	2-7
4-1	Fracture-aperture change ratios applied to define a generic TM-altered zone and the resulting magnification factor for vertical flux across the repository axis	4-1

ACRONYMS

CRWMS M&O	Civilian Radioactive Waste Management System Management and Operating Contractor
DOE	U.S. Department of Energy
EDA-II	Enhanced Design Alternative II
KTI	Key Technical Issue
MTU	Metric Tons of Uranium
RDTME	Repository Design Thermal Mechanical Effects
RMQ1	Lowest Rock-Mass Quality
RMQ5	Highest Rock-Mass Quality
TEF	Thermal Effects on Flow
TH	Thermal-Hydrological
TM	Thermal-Mechanical
VA	Viability Assessment
YM	Yucca Mountain
YMP	Yucca Mountain Project
WP	Waste Package

ACKNOWLEDGMENTS

This report was prepared to document work performed by the Center for Nuclear Waste Regulatory Analyses (CNWRA) for the Nuclear Regulatory Commission (NRC) under Contract No. NRC-02-97-009. The activities reported here were performed on behalf of the NRC Office of Nuclear Material Safety and Safeguards, Division of Waste Management. The report is an independent product of the CNWRA and does not necessarily reflect the views or regulatory position of the NRC.

The author thanks Drs. R. Chen and W. Patrick for their reviews of this report. The author is grateful to J. Wike for assisting with the word processing and preparation of the final report and to B. Long for the editorial review.

QUALITY OF DATA, ANALYSES, AND CODE DEVELOPMENT

DATA: All CNWRA-generated original data contained in this report meet quality assurance (QA) requirements described in the CNWRA QA Manual. Sources for other data should be consulted for determining the level of quality for those data.

ANALYSES AND CODES: Finite element (thermal-mechanical) analyses in this report were conducted using the commercial computer code ABAQUS Version 5.8 and the finite difference (thermal-hydrological) analyses were conducted using the CNWRA-developed MULTIFLO code. ABAQUS and MULTIFLO are controlled under the CNWRA software QA procedure (TOP-018, Development and Control of Scientific and Engineering Software).

1 INTRODUCTION

1.1 BACKGROUND

The host rock mass for the proposed repository at Yucca Mountain (YM) may undergo changes in hydrological properties owing to the geomechanical response of the rock mass to heat generated by radioactive decay of nuclear waste. A change in hydrological properties is important because of potential effects on the amounts of water seepage (percolation flux) through the repository horizon. One design option being considered for the repository relies on the emplacement drifts remaining dry for long periods of time to slow down the corrosion of the waste packages (WPs) and, consequently, delay the release of radionuclides to the environment (U.S. Department of Energy, 1998a). This design option assumes that heat produced by radioactive decay of nuclear waste would vaporize and drive away moisture from the vicinity of the emplacement drifts and prevent moisture return to the resulting dry zones for a long time.

The extent and longevity of such dry zones depend on the thermal load and the percolation flux through the repository horizon. For a given thermal load, the percolation flux determines whether such dry zones may develop, how fast they develop, and how long they remain dry. Intuitively, areas of the repository that receive higher percolation flux will be less likely to experience drying of the emplacement drifts, and the dry zones that develop in such areas will rewet faster than dry zones in areas of lower percolation flux. In addition to its effect on the drying and rewetting of the emplacement drifts, the percolation flux also determines how fast and in what quantities radionuclides may be transported down to the saturated zone after containment failure.

As a result, an understanding of the temporal and spatial distributions of percolation flux through the unsaturated zone is essential to predicting the occurrence and magnitudes of seepage into the emplacement drifts, the onset and rates of WP corrosion, and the transport of radionuclides in aqueous states to the saturated zone. The percolation flux at the repository horizon depends on the net infiltration rate from the ground surface and the hydrological characteristics of the overlying rock units. The time-averaged infiltration rate at YM varies spatially from less than 1 mm/yr to about 40 mm/yr, depending on factors such as soil and vegetation cover and topographic relief (U.S. Department of Energy, 1998b; Hevesi and Flint, 1996; Flint et al., 1996; Bagtzoglou et al., 1996; Stothoff, 1997). The spatial average of the time-averaged infiltration rate lies in the range of 5–15 mm/yr. The hydrological characteristics of the rock units are controlled by the degrees of welding and fracturing. Generally, the welded units have low matrix porosity and permeability but are highly fractured; the nonwelded units have higher matrix porosity and permeability but lower fracture density. Consequently, water flow in the unsaturated zone is fracture dominated in the welded units whereas matrix flow is an important contributor to the overall water flux through the nonwelded units.

Therefore, the characteristics of the welded rock units that may affect the percolation flux are the aperture, continuity, and frequency of fractures. Because the proposed repository horizon lies within welded rock units, there is concern that the fracture attributes important to flow may be altered significantly by thermally driven geomechanical and geochemical processes during the period of regulatory concern (e.g., Geomatrix Consultants, Inc., 1998). All three fracture attributes important to flow may change as a result of thermally driven mechanical deformation (in addition to deformations induced by excavation and potential seismic loading). If mechanical deformation consists mainly of movement on preexisting fractures, as would be expected for an already fractured rock mass, then changes in fracture aperture would be more likely than changes in fracture frequency or continuity. Consequently, the welded and densely fractured rock units

within the influence zone of heat generated from radioactive decay of the emplaced nuclear waste can be expected to experience fracture-aperture changes caused by thermally driven mechanical deformation. A change in fracture aperture can be associated with a corresponding change in fracture porosity, permeability, and, possibly, capillarity.

A change in fracture aperture may result either from an increase or decrease in the fracture-normal stress (normal-deformation response) or from the dilation of an individual fracture or a fracture network owing to fracture slip. The normal-deformation response is considered elastic in that the associated aperture change is generally recoverable upon reversal of the stress change (e.g., Barton et al., 1985; Hsiung et al., 1994). On the other hand, fracture slip and the associated dilation are inelastic processes. Heat generated by repository thermal load is expected to cause an increase in compressive stress because of suppressed thermal expansion of the rock, but the compressive stress will decrease slowly as the heat dissipates. As a result, fractures oriented normal to the thermally induced compressive stresses will experience a decrease in aperture that is expected to recover as the heat dissipates. Furthermore, fracture slip may occur in areas where the shear component of the induced stress is sufficient to overcome the shear resistance of fractures. Such slip may induce slip or separation on other fractures, and the associated dilation (fracture-aperture increase) is not reversible.

This report documents the results of a series of numerical-model calculations to determine the characteristics of thermally induced fracture-aperture changes and the resulting effects on the distributions of percolation flux at the repository depth. Changes in fracture aperture owing to repository thermal loading were determined from a series of analyses based on a drift-scale finite element model. The effects of the aperture changes on repository-level percolation flux were determined from thermal-hydrological modeling. The following conclusions are presented: (i) closure of vertical fractures and opening of horizontal fractures can be expected in heated zones where the rock-mass response is dominantly elastic, but the associated fracture-aperture change is small and would not have a significant effect on moisture flow; (ii) fracture dilation can be expected in spatially discontinuous zones [referred to hereafter as the thermal-mechanical (TM) altered zones] within the vicinity of the emplacement drifts and near the middle of the interdrift pillar; (iii) the TM-altered zones would be characterized by horizontal-fracture dilation in areas of high rock-mass quality and vertical-fracture dilation in areas of low rock-mass quality; (iv) the resulting magnitude of permeability increase would be greater around the drift openings than in the pillars, and would depend on thermal loading, rock-mass mechanical properties, and time-dependent mechanical degradation; (v) lateral flow within the TM-altered zones can be expected and would result in redistribution of percolation flux at the repository depth, with elevated vertical flux within and at the downstream end of the altered zones; and (vi) parts of an emplacement drift close to the downstream end of a TM-altered zone can be expected to experience elevated percolation flux.

1.2 U.S. DEPARTMENT OF ENERGY PREDICTIONS OF THERMAL-MECHANICAL EFFECTS ON HYDROLOGICAL PROPERTIES

The U.S. Department of Energy (DOE) concluded that “thermal loading will produce negligible changes in rock hydrologic properties,” promising that the technical bases for the conclusion will be provided in the Near-Field Environment and Engineered Barrier System Process Model Reports.¹ This conclusion is based on numerical modeling performed by Berge et al. (1998, 1999), from which it was concluded that

¹Barr, D. *Thermal Effects on Flow. Presentation at DOE/NRC Technical Exchange on Yucca Mountain Pre-Licensing Issues*. Las Vegas, NV: U.S. Department of Energy, Yucca Mountain Site Characterization Office. April 2000.

(i) slip on a single vertical-fracture set can cause the permeability of the set to increase by a factor of two or less and (ii) if slip occurs simultaneously on two orthogonal sets of vertical fractures, the permeability of the sets can increase by a factor of four or less. The analyses did not detect slip on horizontal fractures, implying that change in horizontal-fracture permeability would not be expected.

The lack of horizontal-fracture slip in the Berge et al. (1998, 1999) model is inconsistent with results obtained by other investigators (e.g., Ahola et al., 1996; Nuclear Regulatory Commission, 1999; Chen et al., 2000). Analyses based on continuum rock-mass modeling have shown that, because of the tabular shape of the proposed emplacement area at YM (horizontal dimensions of approximately 1,200 and 3,000 m and a vertical dimension smaller than 10 m), thermal loading is expected to cause a large increase in horizontal compressive stress and a decrease (by a smaller magnitude) in the vertical compressive stress (e.g., Nuclear Regulatory Commission, 1999). As a result, principal compressive stresses during the thermal regime would be horizontal for the maximum and vertical for the minimum, with the orientation of the maximum principal stress shifting from approximately north-south to approximately east-west. These stress states would favor slip on near-horizontal fractures that may vary in strike from east-west to north-south. Discontinuum rock-mass modeling also identified slip on near-horizontal fractures to be an essential aspect of the anticipated geomechanical response at the proposed repository (e.g., Chen et al., 2000). Therefore, it is surprising that the Berge et al. (1998, 1999) model did not detect slip on subhorizontal fractures.

The analysis procedure used by Berge et al. (1998, 1999) consists of two steps:

- TM analyses of a linear-elastic and isotropic medium to obtain stress distributions
- Postprocessing of the stresses using the Mohr-Coulomb failure criterion for fractures to identify locations at which slip may occur on any of two vertical- and one horizontal-fracture sets. Each slip location identified was assigned a fracture-permeability change ratio of 2 if slip was detected on a single fracture set, or 4 if slip was detected on two orthogonal fracture sets. Fracture-permeability change ratio was defined as $\Delta k/k_o$, where Δk is the fracture-permeability change relative to an initial fracture permeability, k_o . The $\Delta k/k_o$ values of 2 and 4 were considered upper-bound values based on an analysis by Blair (in Hardin, 1998).

Information obtained from the current study shows that the fracture-permeability change ratio associated with rock-mass response to thermal loading at the proposed YM repository can be expected to greatly exceed the upper-bound values suggested by Berge et al. (1998, 1999). The analysis of Berge et al. (1998, 1999) is not able to predict upper-bound values for thermally induced fracture-permeability change for several fundamental reasons.

First, a linear-elastic analysis is inappropriate for calculating fracture-permeability change except for situations where fracture behavior is dominated by normal-deformation response. A change in fracture aperture may arise from elastic processes dominated by the normal-deformation behavior of fractures, or from inelastic processes associated with fracture slip or separation. A model has to account for the inelastic processes to provide a basis for evaluating the resulting permeability change. Because the inelastic response of a fractured rock depends on the stress history and the associated material stiffness changes, analysis techniques that assume linear-elastic response are inappropriate for quantitative evaluation of inelastic response and the associated permeability change.

Second, the increase in fracture aperture associated with the inelastic response of fractured rock is a product of the fracture-network characteristics and less dependent on the behavior of individual fractures (e.g., Chen, 1999). As a result, analyses to quantify permeability changes associated with inelastic rock-mass response need to consider the dilation response of the rock mass in continuum modeling (e.g., Ofoegbu, 1999) or model the fracture network explicitly (e.g., Chen, 1999). The bounding values calculated by Berge et al. (1998, 1999) were based on individual-fracture behavior.

Third, the suggestion that $\Delta k/k_o$ is limited to a maximum value of 2 is incorrect even for an individual fracture. This suggestion is based on an analysis of the dilation-versus-shear behavior of individual fractures presented by Blair (in Hardin, 1998). The Blair analysis is inconsistent with the dilation-versus-shear relationship that has been established based on laboratory testing of individual fractures (e.g., Barton et al., 1985; Bandis, 1990; Hsiung et al., 1994), which shows that fracture dilation increases as shear displacement increases. A simple and commonly used form of the relationship gives the magnitude of dilation (i.e., aperture change, Δb) as a linear multiple of shear displacement, u_s , as follows:

$$\Delta b = u_s \tan \psi_1 \quad (1-1)$$

where ψ_1 is the dilation angle for a single fracture. As a result of this relationship, Δb and, therefore, Δk increase as u_s increases. Laboratory data from Maini and Hocking (in Barton et al., 1985) and model calculations from Barton et al. (1985) indicate $\Delta k/k_o = 100$ at $u_s = 6$ mm and a potential for greater values of $\Delta k/k_o$ as u_s increases. Blair (in Hardin, 1998) assumed that $\Delta u_s/u_{s_o} = 1$ to derive the suggested upper-bound value of 2 for $\Delta k/k_o$, where Δu_s is the shear-displacement increment owing to thermal loading and u_{s_o} is the preexisting shear displacement on the same fracture (e.g., from excavation). No explanation was offered for the assumption of $\Delta u_s/u_{s_o} = 1$ [Blair (in Hardin, 1998); Berge et al., 1998]. The ratio $\Delta u_s/u_{s_o}$ is actually unbounded (may vary from zero to infinity) because the large change in stresses caused by thermal loading (e.g., Nuclear Regulatory Commission, 1999) implies that thermally induced fracture slip at several locations may be superimposed on essentially zero preexisting fracture slip. Therefore, the assumption of $\Delta u_s/u_{s_o} = 1$ is incorrect and may explain why the bounding value for $\Delta k/k_o$ suggested by Berge et al. (1998, 1999) is so inconsistent with the observed behavior of single fractures [e.g., Maini and Hocking in Barton et al. (1985)].

Fourth, the aperture-versus-permeability relationship for individual fractures was incorrectly applied to fracture sets in the analysis by Blair (in Hardin, 1998). For individual fractures,

$$k = \frac{b^2}{12} \quad (1-2)$$

where b is the fracture aperture. On the other hand, the fracture-set permeability, k_p , for a set of fractures characterized by spacing d is (cf. Elsworth and Mase, 1993)

$$k_f = \frac{b^3}{12d} \quad (1-3)$$

which gives the relationship

$$\frac{\Delta k_f}{k_{f_0}} = 3 \left[\frac{\Delta b}{b_0} + 2 \left(\frac{\Delta b}{b_0} \right)^2 + \left(\frac{\Delta b}{b_0} \right)^3 \right] \quad (1-4)$$

where Δk_f is the change in fracture-set permeability relative to an initial value of k_{f_0} , and b_0 is the initial fracture aperture. The assumption $\Delta k_f/k_{f_0} = \Delta k/k_0 = (\Delta b/b_0)^2$ used in Blair's analysis (in Hardin, 1998) is incorrect and would underestimate the permeability change of a fracture set.

2 DESCRIPTION OF MODEL

Numerical modeling was used to examine fracture-aperture changes associated with TM response at the proposed YM repository and the effects of the fracture-aperture changes on repository-level percolation flux. The magnitudes and distributions of fracture-aperture changes were obtained through TM modeling, and the effects of such changes on percolation flux were examined through separate thermal-hydrological (TH) modeling. The TH analyses are described in detail in a separate publication (Ofoegbu et al., 2000), but aspects of the results are presented later in this report. TM modeling focused on the evaluation of fracture dilation associated with inelastic rock-mass response. Fracture-aperture changes associated with elastic rock-mass response can be expected, but the magnitudes are small and can be bounded using field and laboratory test data. A procedure for obtaining upper-bound values of elastic fracture-aperture changes is discussed later.

An approach based on continuum modeling is presented for the evaluation of fracture dilation. Results from the continuum model are complemented with results from a parallel discontinuum model to characterize the TM-altered zones and the fracture-aperture changes that define the altered zones. Fracture dilation is caused by a combination of inelastic processes, such as fracture slip and separation (e.g., Chen, 1999), and is controlled by characteristics of the fracture network. Therefore, the magnitude of dilation is determined by the fracture-network characteristics (such as kinematic relationships between rock blocks) and is less dependent on the properties of individual fractures. Fracture dilation may be represented as a continuum property of the rock mass quantified through the bulk rock-mass dilation angle ψ_b (distinguished from ψ_1 , the dilation angle for a single fracture). The problem with this definition of rock-mass dilation is that ψ_b is difficult, if at all possible, to measure. But the values of ψ_b reasonably can be bounded. Its minimum value of zero applies to a rock mass with a series of parallel and perfectly smooth fractures, such that slip on a given fracture occurs without dilation and would not trigger slip or separation on other fractures. The upper limit of ψ_b is difficult to determine. If inelastic-response analysis is based on plasticity theory, as is often the case (e.g., Ofoegbu and Curran, 1992), then the theory provides an upper limit for ψ_b defined by $\psi_b = \phi$, where ϕ is the friction angle. The physical meaning of this upper limit for ψ_b may be difficult to establish, but it has a firm theoretical basis: the range of behavior for geologic materials defined through plasticity-based modeling varies from nondilatant with $\psi_b = 0$ to associative with $\psi_b = \phi$ (e.g., Hibbit, Karlsson & Sorensen, Inc., 1998).

Therefore, the ratio ψ_b/ϕ may be varied between zero and one to examine the sensitivity of predicted response to ψ_b (e.g., Ofoegbu and Ferrill, 1995). The ratio was set to 0.5 in the analyses presented here, and the associated rock-mass dilation was obtained as the inelastic volumetric strain ϵ^N , as described in the following section.

2.1 CONTINUUM MODEL FOR FRACTURE DILATION

Consider a small rock body subjected to a complete cycle of loading and unloading such that all recoverable deformation caused by the loading is recovered during unloading. Let the rock body undergo inelastic (i.e., nonrecoverable) deformation as a result of the loading and unloading cycle, such that its

volume changes from V_{i0} at the beginning of the cycle to V_{i1} at the end. The change in volume is accounted for entirely by a change in fracture-space volume from V_{f0} at the beginning of the cycle to V_{f1} at the end. The inelastic volumetric strain is given by

$$\varepsilon^N = \frac{V_{i1} - V_{i0}}{V_{i0}} = \frac{V_{f1} - V_{f0}}{V_{i0}} = \frac{\Delta V_f}{V_{i0}} \quad (2-1)$$

where $\Delta V_f = V_{f1} - V_{f0}$. The initial and final fracture porosity φ_{f0} and φ_{f1} are given by

$$\varphi_{f0} = \frac{V_{f0}}{V_{i0}} \quad (2-2)$$

$$\varphi_{f1} = \frac{V_{f1}}{V_{i1}} = \frac{V_{f0} + \Delta V_f}{V_{i0} + \Delta V_f} \quad (2-3)$$

The following is obtained by dividing the numerator and denominator of Eq. (2-3) with V_{i0} and using Eqs. (2-1) and (2-2):

$$\varphi_{f1} = \frac{\varphi_{f0} + \varepsilon^N}{1 + \varepsilon^N} \quad (2-4)$$

Because $1 + \varepsilon^N \approx 1$ and $\Delta\varphi_f = \varphi_{f1} - \varphi_{f0}$, Eq. (2-4) gives the relationship between fracture-porosity increment and inelastic volumetric strain as

$$\Delta\varphi_f = \varepsilon^N \quad (2-5)$$

It is assumed that the fracture system in the rock body being considered can be represented by three mutually perpendicular sets, each with spacing d and fracture aperture b . This assumption can be relaxed to allow for different fracture spacing and aperture for each set (cf. Elsworth and Mase, 1993). The assumption of the same spacing and aperture in three mutually perpendicular directions restricts application of the resulting equations to isotropic modeling only. Results from such a model can provide information on the magnitudes of fracture-porosity and permeability change but not on the orientation of the dilating fractures. Information on orientation can be developed, however, from discontinuum modeling (e.g., Chen et al., 2000) as illustrated later. Following the assumption of same spacing and aperture in three mutually perpendicular directions, the linear fracture density (number of fractures per unit length) normal to a given fracture set is $1/d$ and the volumetric fracture density is $3/d$. The fracture aperture changes from b_o to $b_o + \Delta b$, and the fracture porosity from φ_{f0} to $\varphi_{f0} + \Delta\varphi_f$ as a result of inelastic deformation during a loading cycle such as defined previously, where (cf. Snow, 1968)

$$\varphi_{f0} = \frac{3b_o}{d} \quad \text{and} \quad \Delta\varphi_f = \frac{3\Delta b}{d} \quad (2-6)$$

The fracture permeability in a fracture-parallel direction is contributed by two orthogonal fracture sets and given by (Snow, 1968; Elsworth and Mase, 1993)

$$k_f = \frac{b^3}{6d} \quad (2-7)$$

The initial and final fracture permeabilities k_{fo} and k_{f1} , which correspond to apertures b_o and $b_o + \Delta b$, respectively, can be related through the equation

$$k_{f1} = R_k k_{fo} \quad (2-8)$$

It can be shown using Eqs. (2-6) and (2-7) that the fracture-permeability change ratio R_k is related as follows to the corresponding aperture- and porosity-change ratios, R_b and R_ϕ , respectively:

$$R_k = R_b^3 = R_\phi^3 \quad (2-9)$$

$$R_b = 1 + \frac{\Delta b}{b_o} \quad (2-10)$$

$$R_\phi = 1 + \frac{\Delta \phi}{\phi_o} = 1 + \frac{\varepsilon^N}{\phi_o} \quad (2-11)$$

The accumulated inelastic volumetric strain ε^N from a given loading history can be evaluated through plasticity-based continuum analysis (e.g., Ofoegbu and Curran, 1992), and the corresponding change in fracture porosity, aperture, and permeability can be obtained using Eqs. (2-5) and (2-9) through (2-11).

2.2 MODEL GEOMETRY FOR THERMAL-MECHANICAL ANALYSES

TM analyses were performed using a two-dimensional (plane strain) drift-scale model extending 40.5 m horizontally and 670 m vertically (figure 2-1). The emplacement drift is represented in the model as a vertical semicircle of 5.5-m diameter. The model extends horizontally from the center of the drift to the middle of the interdrift pillar, representing a drift center-to-center spacing of 81 m as specified for the Enhanced Design Alternative II (EDA-II) design (TRW Environmental Safety Systems, Inc., 1999). The part of the domain within 100 m above and below the drift axis was modeled as elastic-plastic using the Mohr-Coulomb strength criterion. Results from previous work (e.g., Ofoegbu, 1999) suggest that inelastic response is not expected outside this zone. Therefore, the part of the domain at more than 100 m above and below the drift axis was modeled as linear elastic.

2.3 BOUNDARY AND INITIAL CONDITIONS

The thermal boundary conditions consist of fixed temperature at the top (ground surface) and base (water table) of the model and zero heat flux normal to the vertical boundaries. The excavated drift was not included in the thermal-analysis model. Instead, a volumetric heat source was applied within material inside the drift perimeter, as explained later. The mechanical boundary conditions are zero vertical displacement

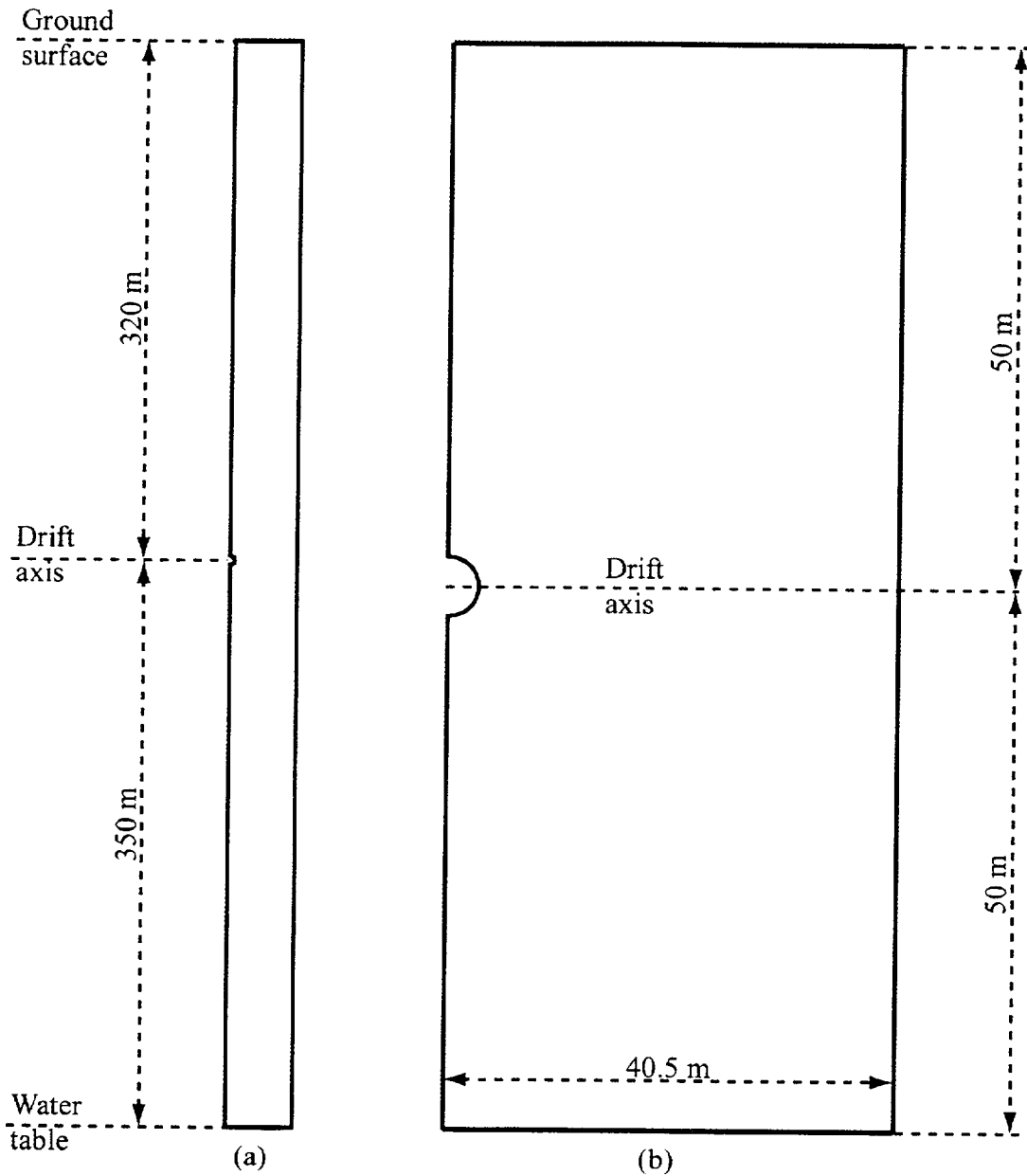


Figure 2-1. Outline of model domain (solid lines) showing (a) full model and (b) part of model within 50 m above and below the drift axis.

at the base, zero horizontal displacement on the vertical boundaries, and free-surface condition at the top. The drift opening was not included in the model at the start, but was introduced by removing materials within the drift perimeter after the initial equilibrium state was established. The drift perimeter was treated as a free surface thereafter. The thermal and mechanical boundary conditions on the vertical boundaries simulate vertical symmetry planes.

Initial temperature was defined using a temperature of 18.7 °C at the ground surface and the geothermal gradient for the site defined in table 2-1 (Civilian Radioactive Waste Management System Management and Operating Contractor, 1997a), which gives a temperature of 34.3 °C at the model base. Initial stress was defined using a depth gradient of approximately 0.022 MPa/m (equivalent to rock density of 2,210 kg/m³ and gravitational acceleration of 9.81 m/s²) for vertical stress and a horizontal-to-vertical stress ratio of approximately 0.266 [obtained from $\nu/(1 - \nu)$, where $\nu = 0.21$ is the Poisson's ratio].

Table 2-1. Yucca Mountain geothermal gradient (Civilian Radioactive Waste Management System Management and Operating Contractor, 1997a)

Depth (m)	Temperature Gradient (°C/m)
0-150	0.02
150-400	0.018
400-700	0.03
> 700	0.008

2.4 THERMAL LOADING

Material inside the drift perimeter was treated as heat-generating rock to simulate heat source from radioactive decay of nuclear waste. The applied source strength is equivalent to 1.226 kW/m of drift at zero time and was decayed with time to 0.0166 kW/m at 10,000 yr following the decay characteristics defined in table V-1 of Civilian Radioactive Waste Management System Management and Operating Contractor (CRWMS M&O) (1997a). This source strength combines with the drift center-to-center spacing of 81 m to give a thermal load equivalent to 60 metric tons of uranium (MTU)/acre, which is the proposed thermal load for the EDA-II design (TRW Environmental Safety Systems, Inc., 1999). The EDA-II design also includes ventilation, but the information required to account for potential effects of ventilation on heat flow has not been developed. Therefore, the effect of ventilation was not included in the model. Ventilation can be expected to result in reduced TM effects, depending on the magnitude of temperature reduction owing to ventilation and the duration during which the reduction occurs.

2.5 THERMAL AND MECHANICAL PROPERTIES

The model was treated as homogeneous and assigned properties of the lower lithophysal unit of the Topopah Spring Welded Tuff [e.g., table 4-3 of CRWMS M&O (1998)]. Rock-mass properties vary both vertically and laterally at YM because of stratigraphic layering and differences in the degree of fracturing and lithophysal content. The effects of such spatial variation of properties can be examined more appropriately through site-scale models large enough to include the property variations (e.g., Ofoegbu, 1999). Spatial variation of properties may also be represented approximately by applying different property sets to a drift-scale model such as described in section 2.2. Results from such drift-scale models should be interpreted in conjunction with site-scale model results to consider potential effects of spatial property gradients, which are not incorporated in the drift-scale model. The drift-scale approach (without a companion

site-scale model) was used in the current analyses with two sets of mechanical properties representing the highest rock-mass quality (RMQ5) and the lowest rock-mass quality (RMQ1) categories. These quality categories were defined by the Yucca Mountain Project (YMP) to account for the effects of varying degrees of fracturing on rock-mass mechanical properties at YM [e.g., CRWMS M&O (1998)].

2.5.1 Thermal Properties

The thermal property values are density, ρ , of 2,210 kg/m³, thermal conductivity, κ , of 2.13 W/m·K, and specific heat capacity, C_m , which varies with temperature as defined in table 2-2 [e.g., CRWMS M&O (1998)]. The temperature-dependent heat capacities in table 2-2 were developed to account for the effects of evaporation and condensation in conduction-only heat transfer models. TH models that explicitly account for coupled heat and mass transfer (e.g., Lichtner et al., 2000) use constant heat capacities that represent the heat-absorption characteristics of the rock without the effects of water phase change. For example, Hardin (1998, table 3-5) gives $C_m = 900$ J/kg·K for the lower lithophysal unit of Topopah Spring Welded Tuff for use in TH analyses. This value of C_m differs from the values in table 2-2 for representing the same rock unit in heat conduction models.

2.5.2 Mechanical Properties

The rock-mass stiffness parameters are [from CRWMS M&O (1998)] Poisson's ratio $\nu = 0.21$; Young's modulus, E , of 7.8 GPa for RMQ1 and 32.6 GPa for RMQ5; and thermal expansivity, α , that varies with temperature as in table 2-3. The values of Mohr-Coulomb rock-mass strength parameters (friction angle ϕ and cohesion c) given in CRWMS M&O (1998) are inconsistent with the rock-mass quality, Q , values of 0.47 for RMQ1 and 9.30 for RMQ5. The values of c and ϕ consistent with these values of Q were determined following the procedure in Hoek and Brown (1997) and are shown in table 2-4 (cf. Nuclear Regulatory Commission, 1999). Intact-rock strength parameters required in the Hoek-Brown procedure were assigned the values shown in table 2-4 [m_i from Brechtel et al. (1995) and σ_{ci} from CRWMS M&O (1997b)].

Table 2-2. Specific heat capacity for the lower lithophysal unit of Topopah Spring Welded Tuff, described as a function of temperature to represent the effects of evaporation in heat conduction analyses (Civilian Radioactive Waste Management System Management and Operating Contractor, 1998)

Temperature (°C)	Specific Heat Capacity (J/kg · K)
≤ 94	968.96
> 94–114	4741.45
> 114	988.19

Table 2-3. Thermal expansivity of Topopah Spring Welded Tuff described as a function of temperature (Civilian Radioactive Waste Management System Management and Operating Contractor, 1998)

Temperature (°C)	Thermal Expansivity (10 ⁻⁶ /K)
0	7.14
50	7.14
100	9.07
125	9.98
150	11.74
175	13.09
200	15.47

Table 2-4. Rock-mass strength parameters obtained using empirical relationships from Hoek and Brown (1997). Unconfined compressive strength of intact rock is reduced to 50 percent of its conventional laboratory value to account for the effects of sustained loading following Lajtai and Schmidtke (1986).

Parameter	RMQ1 Category	RMQ5 Category
Rock mass quality, Q	0.47	9.30
Hoek-Brown intact rock parameter, m_i	10	10
50 percent of intact-rock unconfined compressive strength, σ_{ci} (MPa)	84.0	84.0
Friction angle, ϕ	27.5°	34.4°
Cohesion, c (MPa)	2.82	5.08
Note: RMQ = Rock-mass quality		

The value of σ_{ci} was reduced by 50 percent (table 2-4) to account for the effect of sustained loading on intact-rock strength. It has been demonstrated through laboratory data (e.g., Lajtai and Schmidtke, 1986) that the strength of intact hard rocks (e.g., granite, sandstone, welded tuff) under slow or sustained loading may be much smaller than the strength obtained through conventional (usually rapid) laboratory loading conditions. If loading rate is slow enough, slow-growing fractures, such as driven by stress corrosion at crack tips, have sufficient time to extend and coalesce to cause rupture. Such fractures usually do not have sufficient time to grow under the rapid loading conditions of conventional laboratory compression testing. Consequently, intact-rock strength is considerably smaller under sustained loading than under conventional laboratory loading. For example, Lajtai & Schmidtke (1986) obtained unconfined compressive strength of crystalline igneous rocks under sustained loading that are as low as 60 percent of the conventional

unconfined compressive strength. Because the repository environment will be subjected to mechanical loading arising mainly from suppressed thermal expansion of rock under elevated temperatures that may be sustained for a long time (a few hundred years, at least), the strength of intact rock within the environment should be governed by behavior under sustained loading. Consequently, the unconfined compressive strength of intact rock was set to 50 percent of the value obtained from conventional laboratory testing.

2.5.3 Rock-Mass Degradation from Geochemical Alteration of Fracture-Wall Rock

In addition to the reduced strength of intact rock owing to sustained loading, rock-mass mechanical degradation related to the geochemical response of the system to elevated temperature would be expected. Heat generated from nuclear waste is expected to cause a geochemical response because mineral stabilities and equilibria depend on temperature; geochemical reaction rates in the presence of water would accelerate at elevated temperature; and the thermal gradients would cause redistribution of moisture, solutes, and carbon dioxide, which are essential to the chemical reactions (Murphy, 1993). Reaction-path modeling of the natural gas-water-rock geochemical system at YM (Murphy, 1993) indicates that anticipated geochemical reactions include dissolution of feldspars; precipitation of secondary minerals such as clinoptilolite, smectite, and calcite; and increase in pH and aqueous sodium bicarbonate concentrations. Although the repository-induced mineralogical changes are likely to affect only a small rock volume, the changes are expected to be localized at fluid-rock interfaces, such as fracture walls and lithophysal cavities. Consequently, the alteration minerals would be expected to develop as lithophysal-cavity deposits or fracture coatings.

Mineral-alteration products occur at YM mostly as fracture coating and as lithophysal-cavity deposits (Carlos et al., 1995). The mineralogy, thickness, and amount and uniformity of coverage of fracture coatings are highly variable and uncertain (cf. Thoma et al., 1992). The coatings consist mainly of zeolites, manganese oxide minerals, silica phases, carbonates (mostly calcite), and clay minerals (mostly smectite, but occasionally illite). Smectite is fairly ubiquitous in fractures throughout the volcanic sequence (Carlos et al., 1995). The genesis of the fracture coatings at YM is not well understood, but the coatings are generally secondary minerals formed as alteration products of primary minerals such as glass, feldspar, and silica phases (Murphy, 1993; Carlos et al., 1995; Levy et al., 1996).

If quartz and other silica phases are the dominant fracture coatings (e.g., Lin and Daily, 1984; Daily et al., 1987; Matyskiela, 1997), then the shear strength of fractures and, therefore, the rock-mass strength, can be expected to increase. If, on the other hand, fracture coatings consist mainly of secondary minerals such as smectite and calcite that are mechanically weaker than the primary minerals (Kenney, 1967; Mitchell, 1976, p. 309), a weakening of the fractures and, therefore, the rock mass, can be expected. The secondary minerals would develop either as fracture-wall precipitates from aqueous solutions or in-place alteration products of fracture-wall rock. The result would be a change in the mechanical characteristics of fractures within the affected zone from "rough, irregular, and tightly healed" to "wide and filled with clay minerals (or other alteration products) thick enough to prevent wall-rock contact" (cf. Barton et al., 1974). Such a change may be associated with a decrease in rock-mass strength, stiffness, or both (cf. Ofoegbu, 1999), but there is no known information regarding the magnitudes and rates of anticipated rock-mass mechanical degradation from fracture-wall rock alteration. Results from a proposed study of the Paiute Ridge intrusive complex as a natural analogue of coupled thermal-hydrological-chemical processes at the proposed YM repository (Lichtner et al., 1999) may yield information on mineral alteration rates.

For example, CRWMS M&O¹ postulated a decrease in fracture-surface cohesion from approximately 0.07 to 0.01 MPa during a period of approximately 2,000 yr to represent the effects of asperity degradation on gravity-induced rockfall. A decrease in rock-mass cohesion is also postulated here to examine the potential roles of geochemical wall-rock alteration of fractures on TM-induced effects on hydrological properties. The magnitude, rate, and time period of the postulated change (figure 2-2) were chosen somewhat arbitrarily, but the postulated degradation curve shape derives from an expectation that such changes would begin slowly, accelerate during a time period, and decelerate thereafter. Analyses were performed using the strength-parameter values in table 2-4 with and without the cohesion decay in figure 2-2.

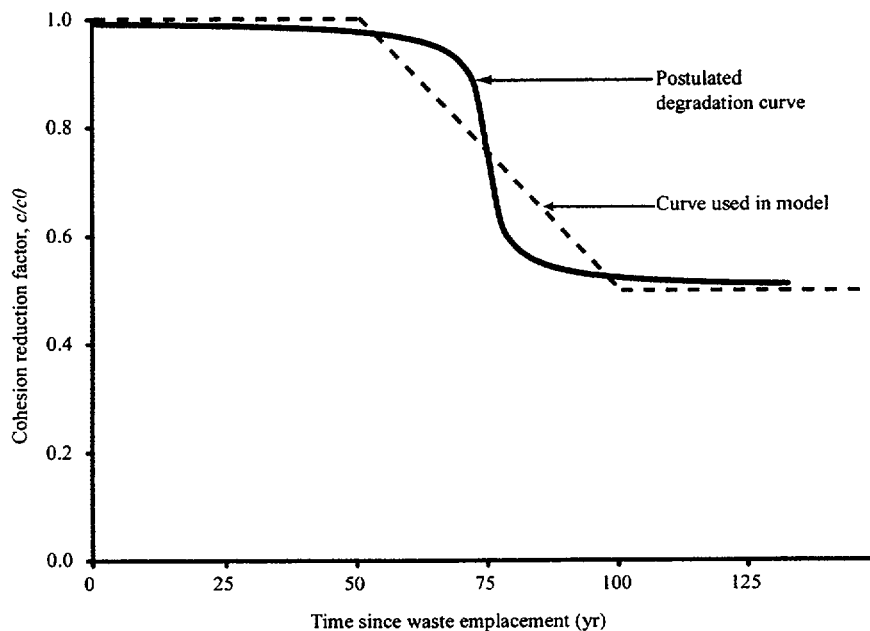


Figure 2-2. Postulated degradation curve for rock-mass cohesion, representing the effects of geochemical alteration of fracture-wall rock. The magnitude, rate, and time period of the postulated degradation were chosen somewhat arbitrarily.

2.6 ANALYSIS PROCEDURE

Analyses of the TM model were conducted using ABAQUS Version 5.8, a commercial finite element code (Hibbit, Karlsson & Sorensen, Inc., 1998). Each analysis consists of a set of sequentially coupled heat-conduction and static stress analyses. The heat conduction analysis was performed for a simulation period of 150 yr from waste emplacement, and the resulting temperature histories were used as input for the associated static stress analysis. Each stress analysis consisted of an initial step to establish the static equilibrium state prior to drift excavation, a second step during which material within the drift perimeter was removed to simulate excavation, and a third and final step during which the temperature histories from the heat conduction analysis were applied to calculate the geomechanical response to the simulated thermal loading. The 150-yr simulation time was chosen to represent early postclosure conditions assuming potential closure of the repository in 50–100 yr.

¹Civilian Radioactive Waste Management System Management and Operating Contractor. *Drift Degradation Analysis. Analysis and Model Report.* ANL-EBS-MD-000027. Revision 00. Las Vegas, NV: Civilian Radioactive Waste Management System Management and Operating Contractor. 1999.

3 ANALYSIS RESULTS

The geometrical and hydrological characteristics of anticipated TM-altered zones are presented based on analysis results from the model described in chapter 2. First, temperature distributions from the thermal analyses are presented. Then, stress distributions from linear-elastic analyses are interpreted in combination with existing data from the literature that indicate the stress conditions under which fracture-aperture changes associated with elastic rock-mass response may be considered negligible. Thereafter, results are presented to illustrate the characteristics of TM effects on fracture permeability and aperture under conditions where rock-mass response is dominantly inelastic.

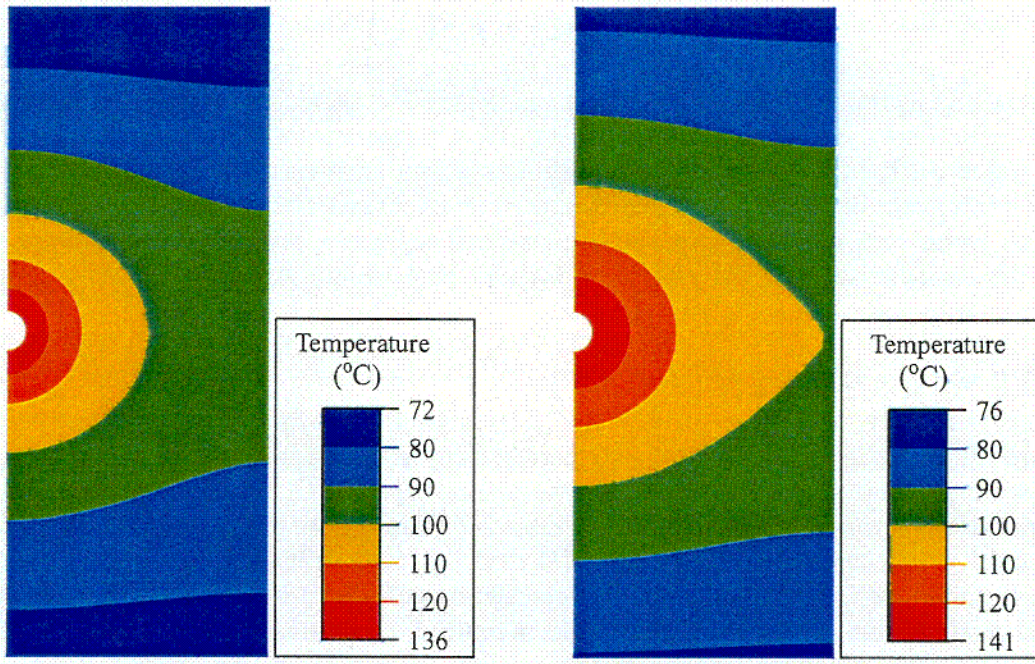
3.1 THERMAL ANALYSIS RESULTS

Figure 3-1 shows temperatures from two thermal-analysis cases: one with the thermal properties described in section 2.5 and a second in which the specific heat capacity, C_m , was set to a constant value of 969 J/kg·K instead of varying with temperature as in table 2-2. Results from this work (e.g., figure 3-1) will in a future study be compared with results from TH modeling to determine if the use of temperature-dependent heat capacities (e.g., table 2-2) in heat conduction analyses provide adequate predictions of repository temperatures for TM modeling. The results in figure 3-1 indicate that the use of a constant heat capacity, compared with temperature-dependent heat capacity, has potentially more effects on temperature gradients and the rock volume within a given isotherm and less on the magnitudes of temperature. For example, the volume within the 100 °C isotherm (figure 3-1) is much larger for the constant heat capacity case than for the temperature-dependent heat capacity case, whereas the drift-wall temperature histories are essentially the same for both cases. Also, the vertical temperature gradient along the 100 °C contour, for example, is noticeably different between the two cases. Temperature distributions from the two cases were used for TM analyses to determine if the temperature differences illustrated in figure 3-1 have significant effects on predicted changes in hydrological properties.

3.2 FRACTURE APERTURE CHANGE FROM ELASTIC ROCK-MASS RESPONSE

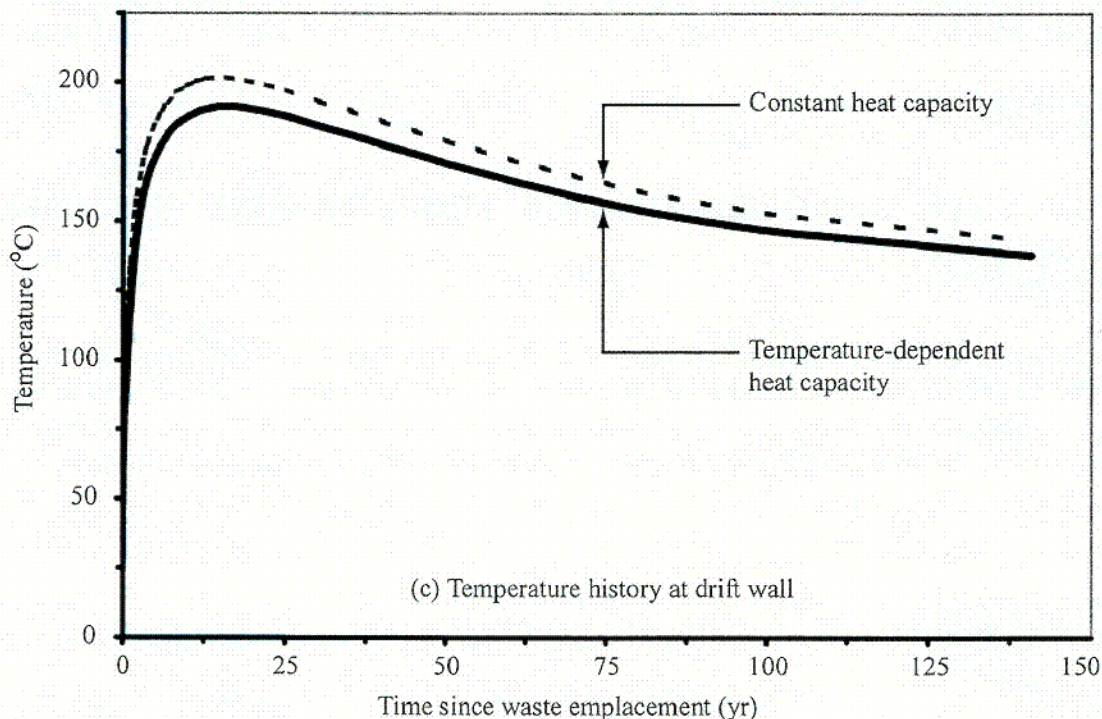
If rock-mass response is dominantly elastic (i.e., if the stress states generally do not satisfy the conditions for inelastic response such as fracture slip or separation), then changes in fracture aperture are controlled by the normal-deformation response of fractures. In such situations, fractures that experience a decrease in normal stress would tend to open, whereas fractures that experience an increase in normal stress would tend to close. The change in fracture aperture, Δb , corresponding to a change in normal stress, $\Delta\sigma_n$, may be calculated using the equation (cf. Bandis et al., 1983; Barton et al., 1985; Hsiung et al., 1994)

$$\Delta b = \frac{A(\sigma_{no} + \Delta\sigma_n)}{1 + B(\sigma_{no} + \Delta\sigma_n)} \quad (3-1)$$



(a) Temperature-dependent heat capacity

(b) Constant heat capacity



(c) Temperature history at drift wall

Figure 3-1. Temperature distributions at 150 yr following waste emplacement for cases with (a) temperature-dependent heat capacity and (b) constant heat capacity. The dimensions and orientation of the plot domain are the same as given in figure 2-1(b). Drift-wall temperature histories also are shown (c) for the two cases.

C01

where A and B are empirical parameters and σ_{no} is the initial normal stress prior to the stress change. Values of A and B depend on σ_{no} and the initial fracture aperture b_o . Consequently, the relationship between laboratory and *in-situ* values of these parameters can introduce considerable uncertainty into predictions of fracture-aperture change from normal-deformation response (Barton et al., 1985; Hsiung et al., 1994). Better estimates of the normal-deformation (more appropriately, aperture-versus-normal stress) response of fractures can be derived from field data such as shown in figure 3-2. The plot, adopted from Wei et al. (1995), was based on data developed originally by Snow (1968) from 5,532 injection tests performed at several dam sites. A wide variety of rock types is represented in the data including granite, gneiss, metavolcanic rocks, slate, phyllite, schists, cemented sandstones, and shale. The calculation of fracture aperture from discharge rates obtained from the injection tests was based on the assumption that the fracture network can be represented in terms of three orthogonal fracture sets, each with uniform fracture spacing d and aperture b (Snow, 1968). As indicated earlier, this assumption enables the fracture porosity and permeability to be related to the aperture and spacing through Eqs. (2-6) and (2-7). The resulting aperture varies with depth following an approximately hyperbolic relationship (figure 3-2).

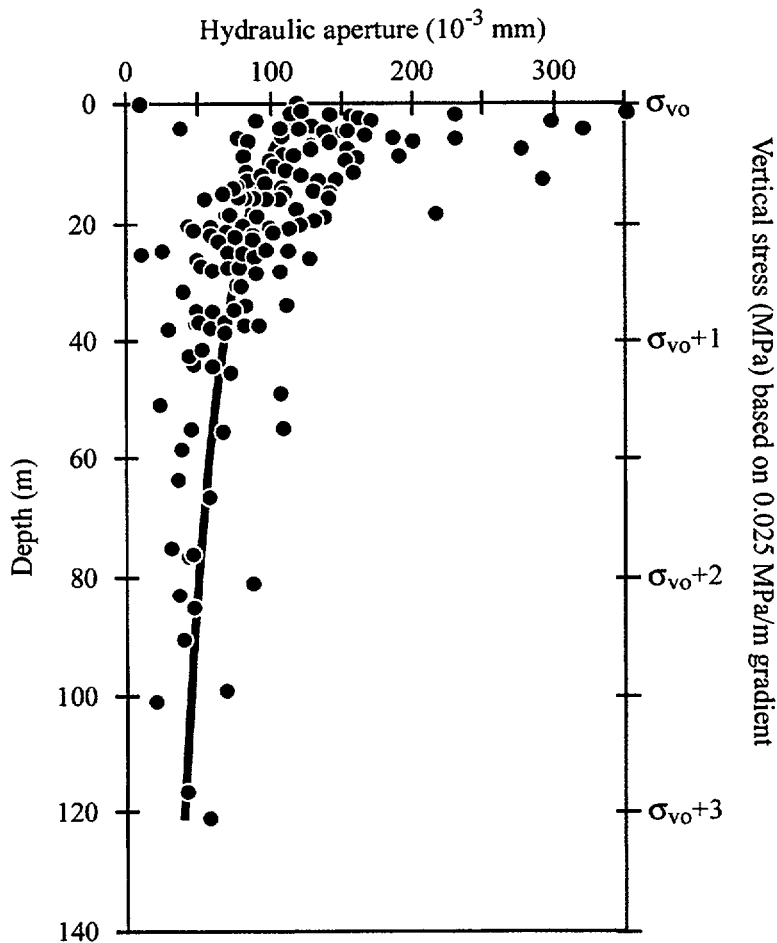


Figure 3-2. Variation of fracture aperture with depth below bedrock surface based on data developed by Snow (1968). A hyperbolic aperture-versus-depth fit by Wei et al. (1995) is shown as solid-line curve. Vertical stress axis was added here based on an assumption of linear increase of stress with depth, with σ_{vo} representing the vertical stress at the bedrock surface.

The hyperbolic aperture-versus-depth relationship implies a hyperbolic relationship between aperture and stress, if stress varies linearly with depth. As Snow (1968) indicated, however, dam sites commonly occupy V-shaped valleys, below which the magnitude and depth-gradient of stress vary laterally. Consequently, the stress conditions at the various sites may depart from the assumption of linear variation of stress with depth. The amount of departure from linear stress-versus-depth relationship is probably small considering that such a relationship would result in a hyperbolic aperture-versus-stress fit to the data, which is consistent with laboratory test results (cf. Bandis et al., 1983; Hsiung et al., 1994). Therefore, the data may be interpreted in terms of stress as suggested by the stress axis in figure 3-2.

Interpreted as an aperture-versus-stress relationship, the data in figure 3-2 suggest a limit stress state representing the boundary between lower stresses at which appreciable fracture-aperture change may result from stress change and higher stresses at which changes in stress would not cause significant change in fracture aperture. If the aperture-versus-stress relationship is represented by two straight lines, the limit stress state would correspond approximately with the stress state at the intersection of the two lines. For the data in figure 3-2, the limit stress state lies at a depth of 10–30 m and is represented by a vertical stress of about $\sigma_{vo}+0.5$ MPa, where σ_{vo} is the vertical stress at the bedrock surface. Laboratory aperture-versus-stress relationships indicate a similar limit, with limit stress states represented by fracture normal stress, σ_n , of about 5–10 MPa (e.g., Bandis et al., 1983). Snow (1968) did not include sufficient information for estimating the value of σ_{vo} . It is, however, unlikely that the overburden depth exceeded about 100 m at any of the dam sites. Therefore, the value of σ_{vo} based on an average stress gradient of 0.025 MPa/m is not likely to exceed about 2.5 MPa, which suggests a limit stress state represented by a vertical stress of about 3 MPa. Changes in stress occurring above this stress state are not likely to cause appreciable change in fracture aperture. More appreciable aperture changes may result from stress changes occurring below the limit stress state.

The initial-stress state at the repository horizon at YM (represented by vertical and horizontal stresses of about 7 and 2 MPa) lies above the limit for appreciable stress-induced fracture-aperture change suggested by the data in figure 3-2. Therefore, an increase in vertical or horizontal stress at YM is not expected to cause an appreciable decrease in fracture aperture. Also, a decrease in stress would not cause an appreciable increase in aperture if the final stress state remains above the limit value. Results in figure 3-3 indicate horizontal stresses increasing everywhere around the emplacement drifts and in the pillars; except in a small area near the drift sidewall and within less than half a drift radius from the sidewall, in which horizontal stress may decrease. This pattern of horizontal-stress distribution is the same in RMQ1 and RMQ5 areas, indicating that the pattern can be expected everywhere irrespective of rock-mass quality variations. Therefore, vertical and near-vertical fractures are not expected to experience appreciable aperture changes from linear-elastic response alone. Figure 3-3 also indicates that vertical stress would increase in the immediate vicinity of the drifts and may increase or decrease in the pillars. The vertical stress magnitude would, however, remain greater than about 5 MPa everywhere, except in an area about two drift diameters large centered at the middle plane of each pillar, within which vertical stresses tend to be small and at times tensile (cf. Nuclear Regulatory Commission, 1999). The vertical-stress characteristic of being greater than about 5 MPa around the drift and at most points in the pillar is consistent through the rock-mass quality range of RMQ1 through RMQ5. The occurrence of a zone of low vertical stress in the pillar appears, however, to be restricted to high rock-mass quality areas. Therefore, horizontal and near-horizontal fractures are not expected to experience appreciable aperture change from elastic response anywhere; except in the low vertical-stress zone where dilation of horizontal and near-horizontal fractures may be expected.

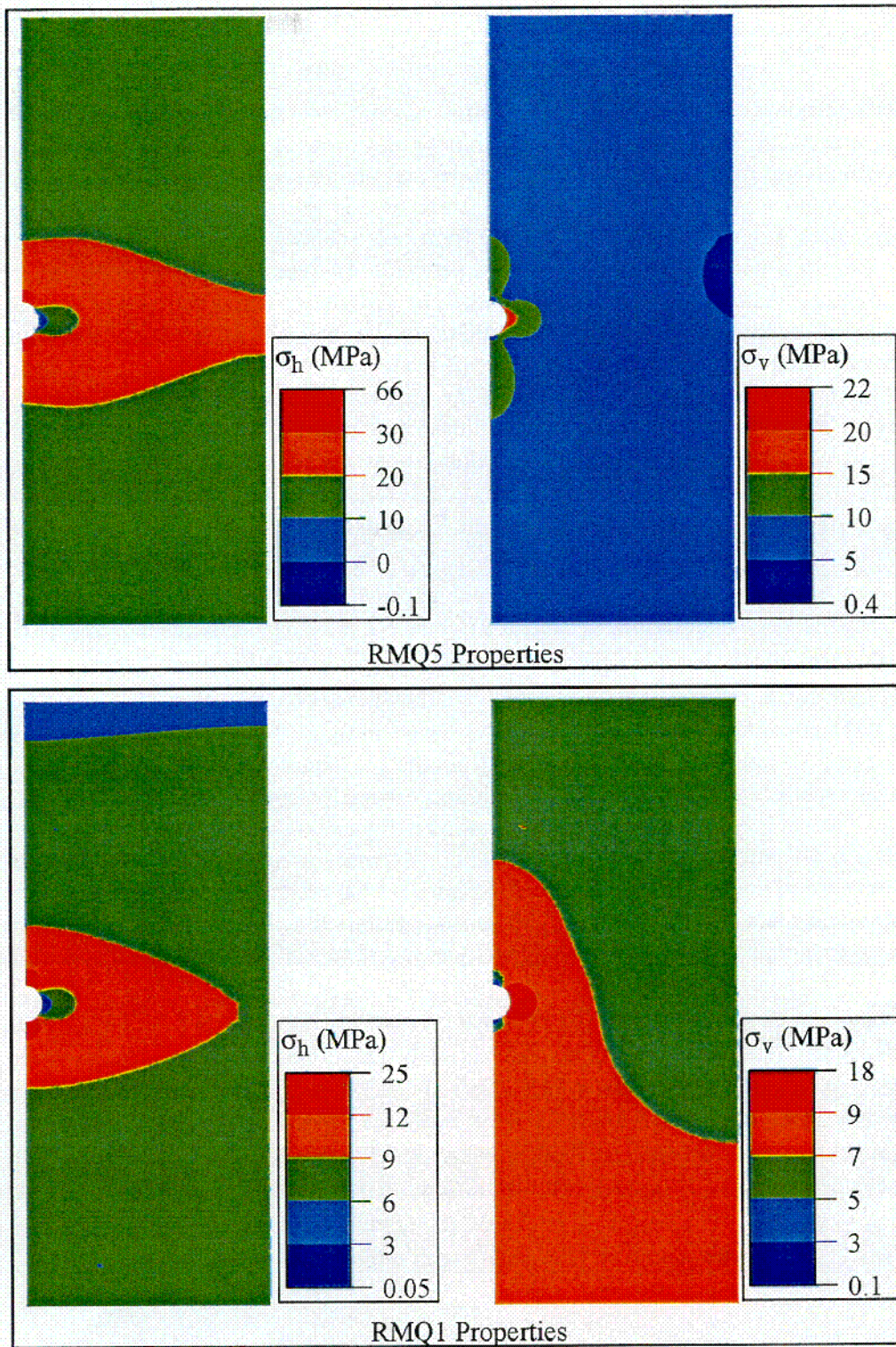


Figure 3-3. Distributions of vertical and horizontal stresses (σ_v and σ_h) at 150 yr following waste emplacement. Results are from linear-elastic analyses, and the dimensions and orientation of the plot domain are the same as in figure 2-1(b).

3.3 FRACTURE PERMEABILITY CHANGE FROM INELASTIC ROCK-MASS RESPONSE

Inelastic response occurs when the induced stress has sufficient shear or tensile components to cause fracture slip or separation. Fracturing of intact-rock blocks may occur also, but the stress conditions for slip or separation of existing fractures are more likely to be met before the conditions for intact-rock failure. Because of the roughness of individual fracture surfaces and the geometrical relationship between neighboring fractures, slip or separation of existing fractures generally causes movement on neighboring fractures resulting in a net dilation of the fracture network. Analyses conducted using the TM model described in chapter 2 indicate two laterally discontinuous TM-altered zones (i.e., zones with $R_k > 1$): one centered at the drift opening and another at the middle of the interdrift pillar. The intensity of fracture dilation, measured using the ratio R_k or R_b [Equations (2-8) through (2-11)], and its spatial extent may vary, depending on thermal loading and TM properties of the rock mass. Values of R_k greater than three orders of magnitude (i.e., R_b greater than one order of magnitude) were obtained. The TM-altered zone centered at the drift generally has greater values of R_k than the altered zone in the pillar.

3.3.1 Effects of Specific Heat and Thermal Expansivity

The specific heat capacity, C_m , and thermal expansivity, α , are both given as functions of temperature, T , by the YMP as described in chapter 2 (tables 2-2 and 2-3). Consequently, the R_k distribution in figure 3-4(d) represents the basecase distribution considering only the effects of C_m and α . The basecase is compared with cases representing three other combinations of constant α ($10^{-5}/K$), constant C_m (969 J/kg·K), and temperature-dependent C_m and α , as shown in figure 3-4. A comparison of cases (a) and (c) or cases (b) and (d) indicates that changing C_m from the constant value to the temperature-dependent function has a strong effect on the predicted R_k distribution, especially for the altered zone at the pillar center. This pattern of C_m effect is consistent with the observation in figure 3-1 that the difference between constant and temperature-dependent C_m has the greatest effect on temperatures and temperature gradients near the pillar center. Because of the difference illustrated in figure 3-4 between corresponding cases with constant and temperature-dependent C_m , the basis for C_m versus temperature functions such as table 2-2 may need to be reexamined to ensure that the amount of heat loss by evaporation is not overestimated by such functions.

A comparison of cases (a) and (b) or cases (c) and (d) indicates that a change in α from a temperature-dependent function to a constant, which is equivalent to decreasing the gradient $\partial\alpha/\partial T$, has the effect of decreasing the predicted R_k values. This effect of $\partial\alpha/\partial T$ may be important considering that the α values provided by DOE (e.g., table 2-3) are for intact rock. *In situ* thermal expansion measurements from the DOE single-heater and drift-scale tests¹ indicate that $\partial\alpha/\partial T$ values for rock mass may be significantly greater than the intact rock values. Consequently, the differences between corresponding cases with constant and temperature-dependent α in figure 3-4 can be interpreted to mean that TM effects on fracture permeability would be underestimated by using intact-rock α instead of rock-mass α .

¹Datta, R. *In Situ* testing. Presentation at DOE/NRC Appendix 7 Meeting on Ground Control. Las Vegas, NV: U.S. Department of Energy, Office of Civilian Radioactive Waste Management. November 1999.

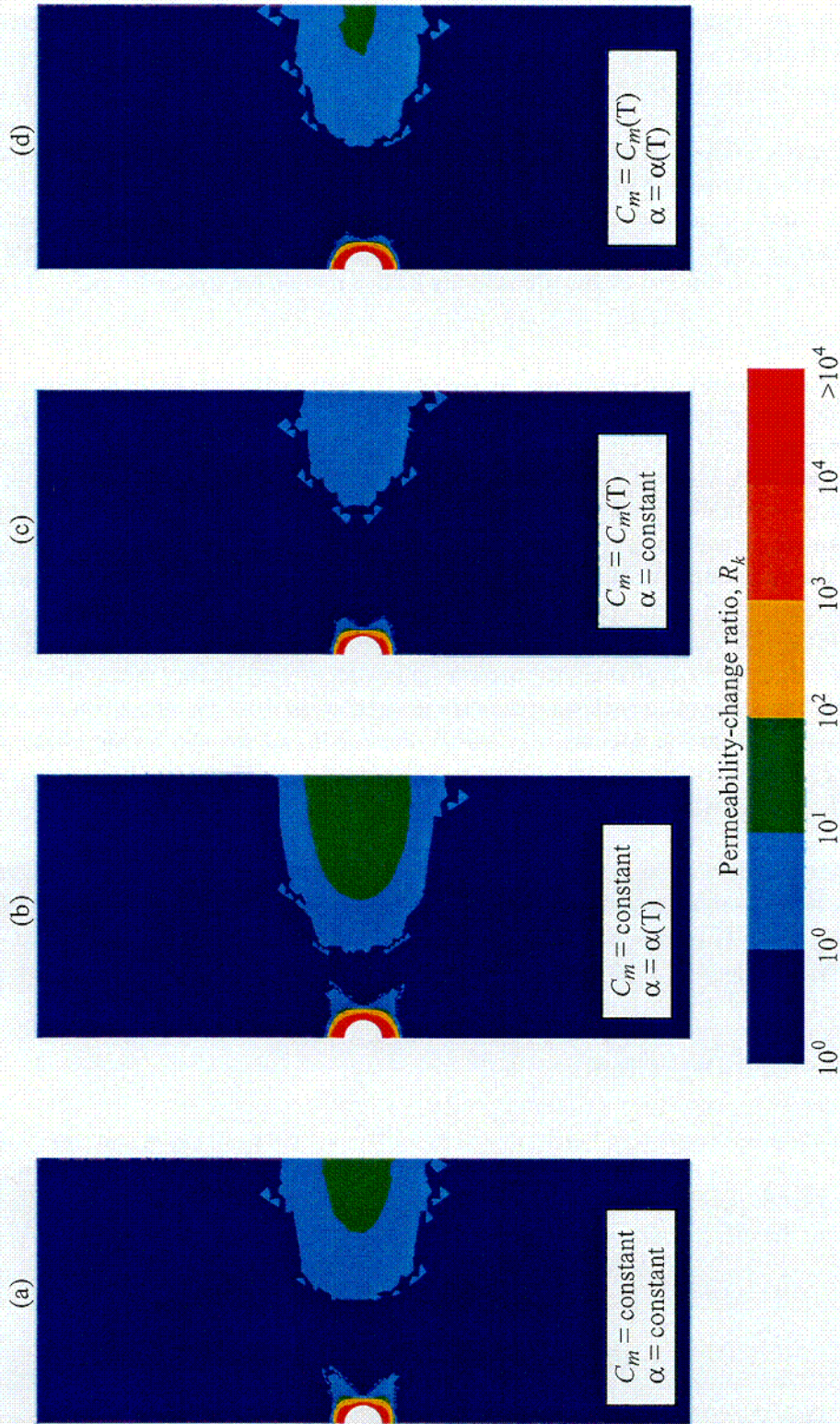


Figure 3-4. Distributions of fracture-permeability change ratio R_k at 150 yr following waste emplacement. The results represent changes associated with inelastic response in RMQ5 areas and illustrate the effects of specific heat capacity C_m and thermal expansivity α , specified either as constants or as functions of temperature, T . The dimensions and orientation of the plot domain are the same as in figure 2-1(b).

3.3.2 Effects of Rock-Mass Quality

The distributions of R_k obtained using basecase TM properties (section 2.5) are presented in figure 3-5 to illustrate the effects of rock-mass quality and time-dependent mechanical degradation. Inelastic response and the associated fracture-permeability change occur near the drift and in the pillars in high rock-mass quality areas, but only near the drift in low rock-mass quality areas. This pattern of inelastic response results in more extensive TM-altered zones in areas of higher rock-mass quality, which is consistent with results reported previously (Ofoegbu, 1999; Nuclear Regulatory Commission, 1999). A similar pattern of response also has been obtained from discontinuum modeling, which provides for explicit representation of fractures in TM calculations (e.g., Chen et al., 2000). For example, results in figure 3-6 indicate the occurrence of fracture slip near the drift and in the pillars in the RMQ5 model, but only near the drift in the RMQ1 model.

As figure 3-6 shows, slip occurs predominantly on subhorizontal fractures in high rock-mass quality areas and on subvertical fractures in low rock-mass quality areas. Inelastic response is stress controlled in high rock-mass quality areas. As noted earlier (section 1.1) the maximum and minimum principal compressive stress components are expected to be horizontal and vertical, respectively, throughout the thermal regime. This stress orientation would favor slip on gently ($\leq 30^\circ$) dipping fractures as illustrated for thrust-faulting conditions in Jaeger and Cook (1979, p. 426). The relatively high stresses in high rock-mass quality areas may satisfy the conditions for slip depending on the strength properties, resulting in stress-controlled inelastic response near the openings and in the pillars as shown in figures 3-5 and 3-6 and in previous work (Ofoegbu, 1999; Nuclear Regulatory Commission, 1999; Chen et al., 2000). Because of small rock-mass stiffness (based on currently available information) in low rock-mass quality areas, stresses are not high enough to cause stress-controlled inelastic response in such areas. But the stress conditions on vertical and subvertical fractures near the opening may satisfy the conditions for slip on such fractures, resulting in structure-controlled inelastic response as shown in figures 3-5 and 3-6 and in previous work (Ofoegbu, 1999; Nuclear Regulatory Commission, 1999; Chen et al., 2000).

The effect of rock-mass stiffness on inelastic response in low rock-mass quality areas is illustrated in figure 3-7, which shows the result of increasing the Young's modulus for RMQ1 to 20 GPa from the 8 GPa currently recommended by DOE (Civilian Radioactive Waste Management System Management and Operating Contractor, 1998). As figure 3-7 shows, such a change would cause increased inelastic response and, consequently, extension of TM-altered zones into the pillars.

3.3.3 Effects of Mechanical Degradation

Mechanical degradation was represented in the model by a fifty-percent decrease in cohesion during a period of approximately 100 yr, as illustrated in figure 2-2. Such a decrease in rock-mass cohesion is relatively modest compared to an approximately 86 percent decrease in fracture-surface cohesion applied by CRWMS M&O¹ to represent the effects of asperity degradation on gravity-induced rockfall. The effects

¹Civilian Radioactive Waste Management System Management and Operating Contractor. *Drift Degradation Analysis. Analysis and Model Report*. ANL-EBS-MD-000027. Revision 00. Las Vegas, NV: Civilian Radioactive Waste Management System Management and Operating Contractor. 1999.

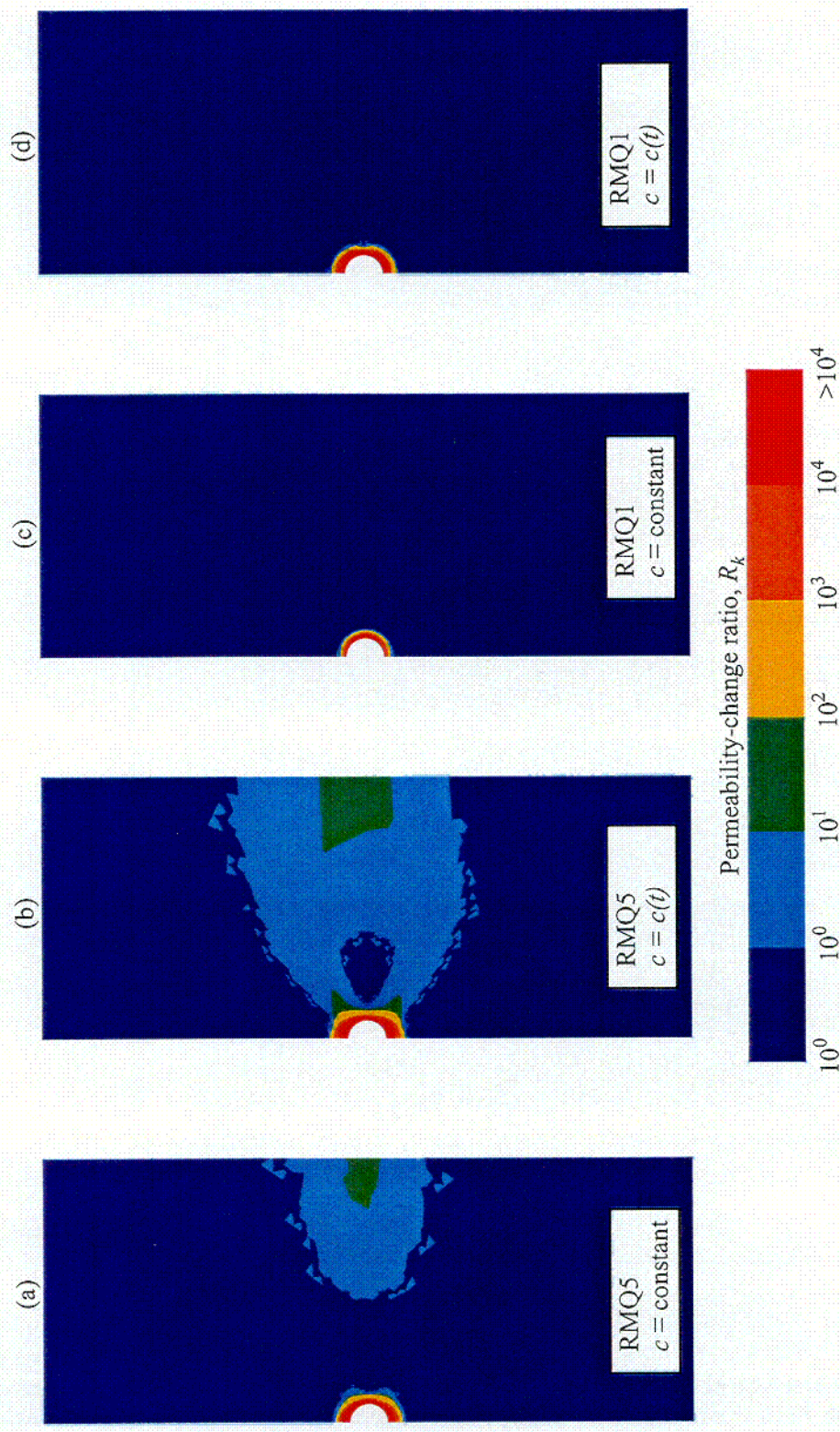
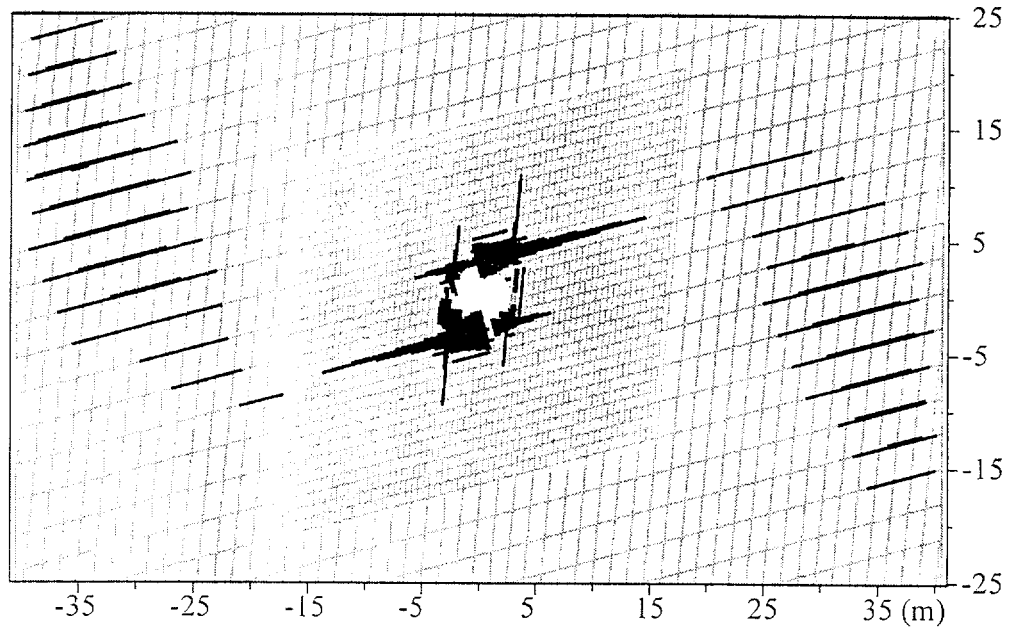
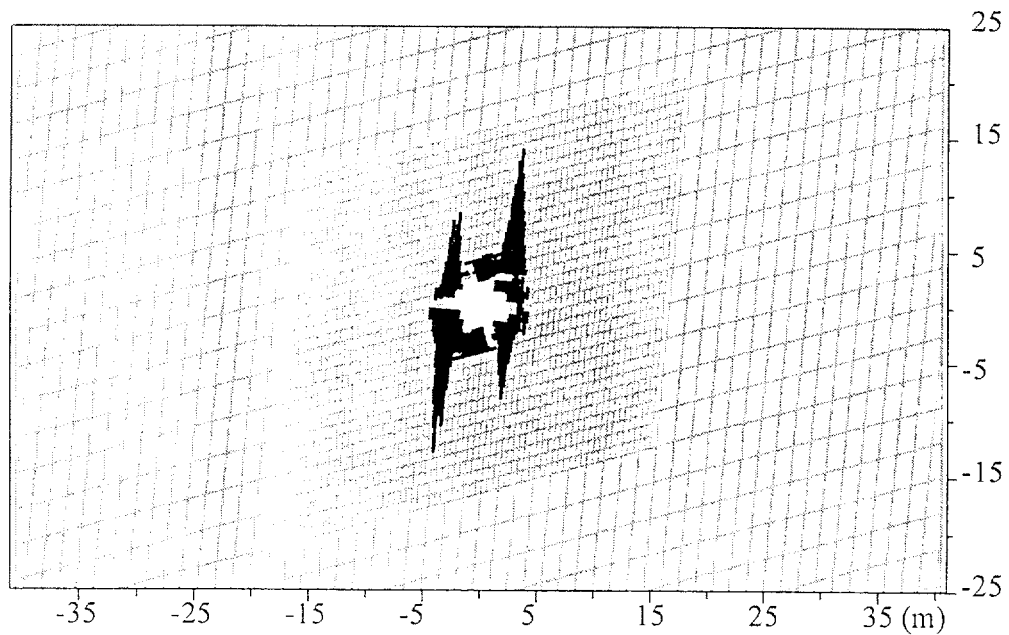


Figure 3-5. Effects of rock-mass quality and mechanical degradation on distributions of fracture-permeability change ratio R_k associated with inelastic response at 150 yr following waste emplacement. The dimensions and orientation of the plot domain are the same as in figure 2-1(b).



(a) RMQ5



(b) RMQ1

Figure 3-6. Discontinuum model results showing the effects of rock-mass quality on distributions of fracture slip at 150 yr following waste emplacement (from Ofoegbu et al., 2000). RMQ5 represents the highest rock-mass quality and RMQ1 represents the lowest. Dotted lines represent individual fractures and the thickness of dark lines is proportional to shear displacement. A detailed discussion of the discontinuum model is given in Chen et al. (2000).

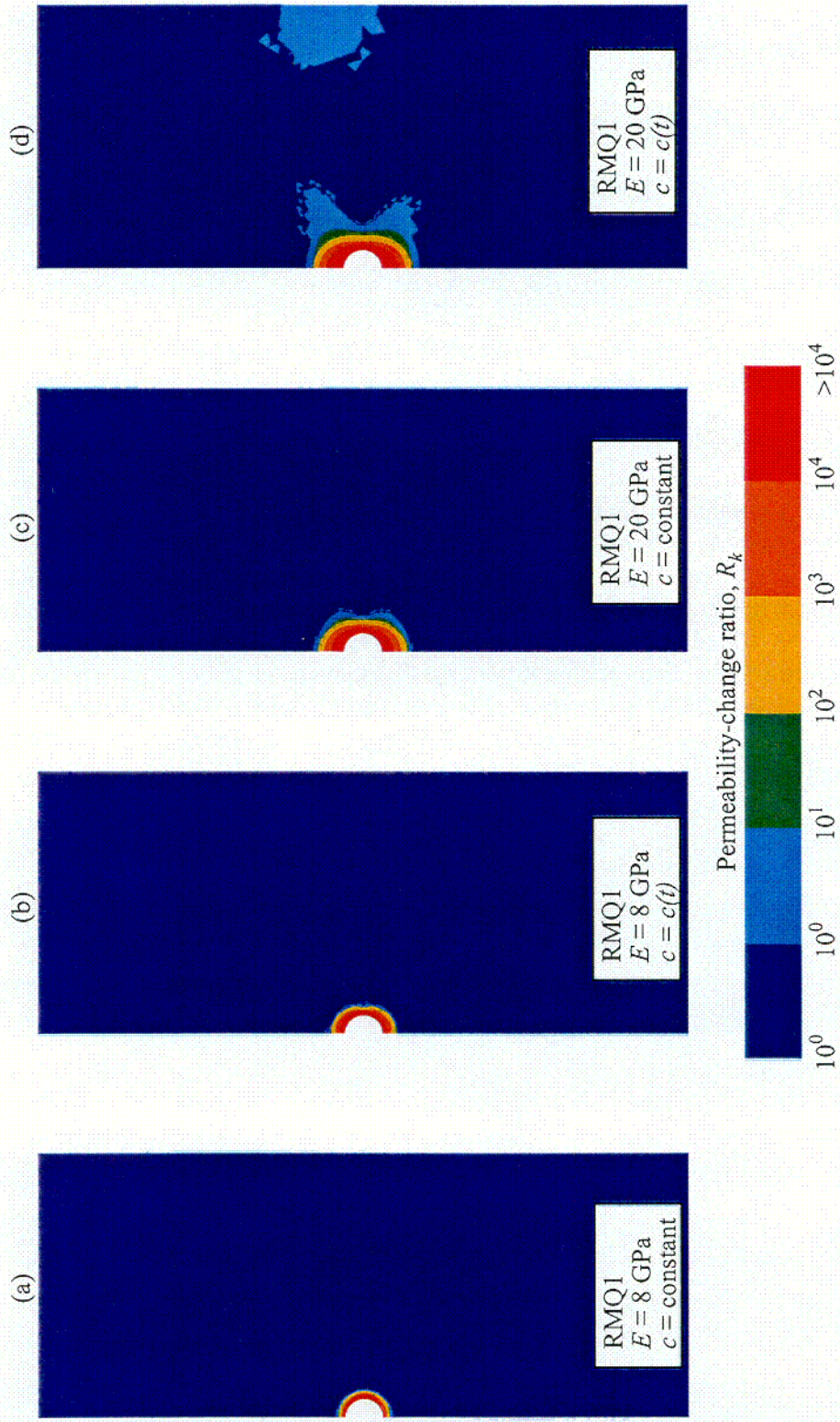


Figure 3-7. Effects of rock-mass stiffness on distributions of fracture-permeability change ratio R_k associated with inelastic response in RMQ1 areas at 150 yr following waste emplacement. The dimensions and orientation of the plot domain are the same as in figure 2-1(b).

on inelastic response and fracture-permeability change are, however, quite significant especially in high rock-mass quality areas [compare figures 3-5(a) and (b)]. The effects in low rock-mass quality areas also may be important [compare figures 3-7(c) and (d)]. In every case, mechanical degradation of the rock mass would result in increased inelastic response and, consequently, growth of TM-altered zones.

3.3.4 Effects of Thermal Loading

Results obtained using a site-scale model based on the viability assessment (VA) design (figure 3-8) illustrates potential effects of higher thermal load on TM-altered zones. A key difference between the VA design (U.S. Department of Energy, 1998c) and the EDA-II design (section 2-2) is the drift center-to-center spacing of 28 m for the VA and 81 m for the EDA-II, which, combined with other differences such as in the indrift WP spacing, give thermal-loading equivalents of 85 MTU/acre for the VA and 60 MTU/acre for the EDA-II. Therefore, the results in figure 3-8 may be compared with the results presented in sections 3.3.1 through 3.3.3, to indicate the effects of higher thermal load. Like the results presented in sections 3.3.1 through 3.3.3, figure 3-8 indicates the occurrence of more extensive TM-altered zones and greater increase in permeability in areas of higher rock-mass quality. As shown in Nuclear Regulatory Commission (1999, figure 5), rock-mass quality, Q , varies laterally in the model from drift number 1 at the north end to drift number 100 at the south end. The value of Q is greatest in the areas around drift numbers 35–53 and 62–70 (with Q values of approximately 5–14) and smaller elsewhere. Mechanical properties vary with Q (Ofoegbu, 1999; Nuclear Regulatory Commission, 1999) and are consistent with the RMQ1 ($Q = 0.47$) and RMQ5 ($Q = 9.30$) properties discussed in section 2.5.2. The areas of relatively extensive altered zones around drift numbers 34–54 (figure 3-8) correspond with areas of relatively high rock-mass quality. An important feature of the R_k distribution in figure 3-8 that distinguishes it from the distributions in earlier figures is the lateral continuity of the $R_k = 10$ –100 zone in high rock-mass quality areas (drift numbers 34–54) of figure 3-8. As shown in figure 3-5, the $R_k = 10$ –100 zones from the EDA-II design model are laterally discontinuous at 150 yr following waste emplacement. Therefore, these results indicate that increased thermal loading would cause TM-altered zones to coalesce earlier, especially in areas of higher rock-mass quality.

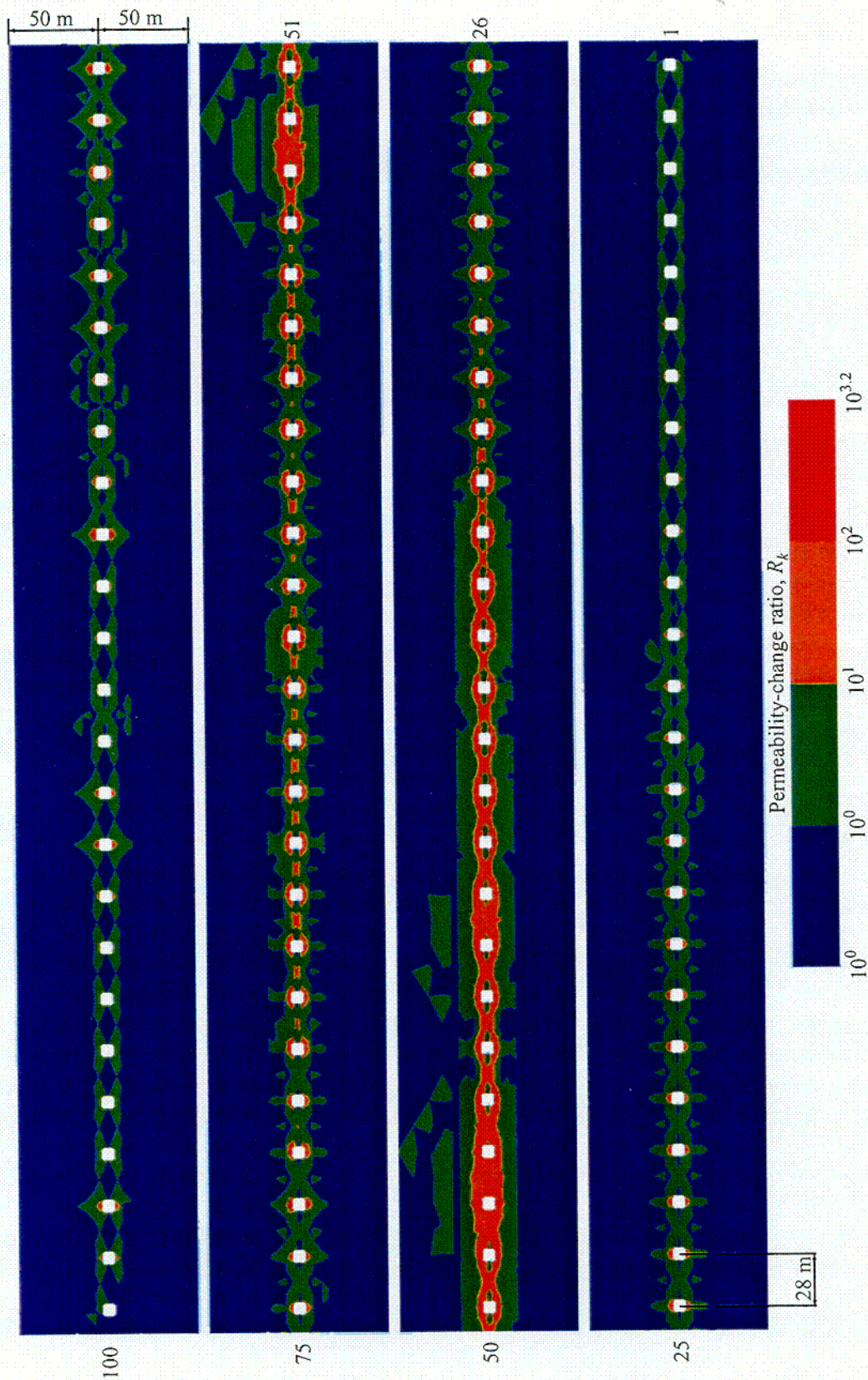


Figure 3-8. Distribution of fracture-permeability change ratio R_k associated with inelastic response at 150 yr following waste emplacement, from a site-scale model based on the viability assessment design. White squares represent emplacement drifts, numbered 1 through 100 from north to south. Model description is given in Ofogbu (1999).

4 EFFECTS OF THERMAL-MECHANICAL-ALTERED ZONES ON MOISTURE FLOW

A series of TH analyses was performed using a site-scale model (figure 4-1) to examine the effects of a generic, laterally discontinuous TM-altered zone on moisture flow. Analyses were performed for a net ground-surface infiltration rate of 10 mm/yr. Thermal-hydrological behavior was simulated using the mass and energy transport module of the thermal-hydrological-chemical simulation system MULTIFLO (Lichtner et al., 2000). A detailed description of the TH model and analysis procedures is given in Ofoegbu et al. (2000). As shown in table 4-1, analyses were performed for a wide range of fracture-aperture change ratios R_b (R_{bh} for horizontal fractures and R_{bv} for vertical fractures), including values representing larger than anticipated vertical-fracture closure. Fracture permeabilities consistent with the modified fracture apertures were determined using Eqs. (2-8) and (2-9).

In all cases, fracture dilation or closure resulted in a redistribution of vertical flux within the altered zone (figures 4-2 and 4-3). Vertical flux is reduced at the upstream (or up-dip) end and increased at the downstream (or down-dip) end of the altered zone, indicating lateral diversion of flux within the altered zone. Closure of vertical fractures would cause flux to be diverted to the outside of the altered zone (figure 4-2, bottom plot), whereas horizontal-fracture dilation tends to cause development of an area of elevated flux within and on the downstream side of the altered zone (figure 4-2, top plot). A fracture-aperture change smaller than about one-half order of magnitude (i.e., $R_b < 10^{0.5}$ for dilation or $R_b > 10^{-0.5}$ for closure) is not likely to produce an appreciable effect on percolation flux (figure 4-2). Larger aperture changes (e.g., $R_b = 10$ for dilation or $R_b = 0.1$ for closure) are likely to cause an appreciable increase in vertical flux near the downstream end of the altered zone.

Table 4-1. Fracture-aperture change ratios applied to define a generic TM-altered zone and the resulting magnification factor for vertical flux across the repository axis

R_{bh}	R_{bv}	Flux Magnification
1.0	10^{-1}	4.0
1.0	$10^{-0.5}$	1.5
$10^{0.5}$	1.0	1.25
10.0	10^{-1}	2.5
10.0	1.0	2.25
10.0	10.0	1.25

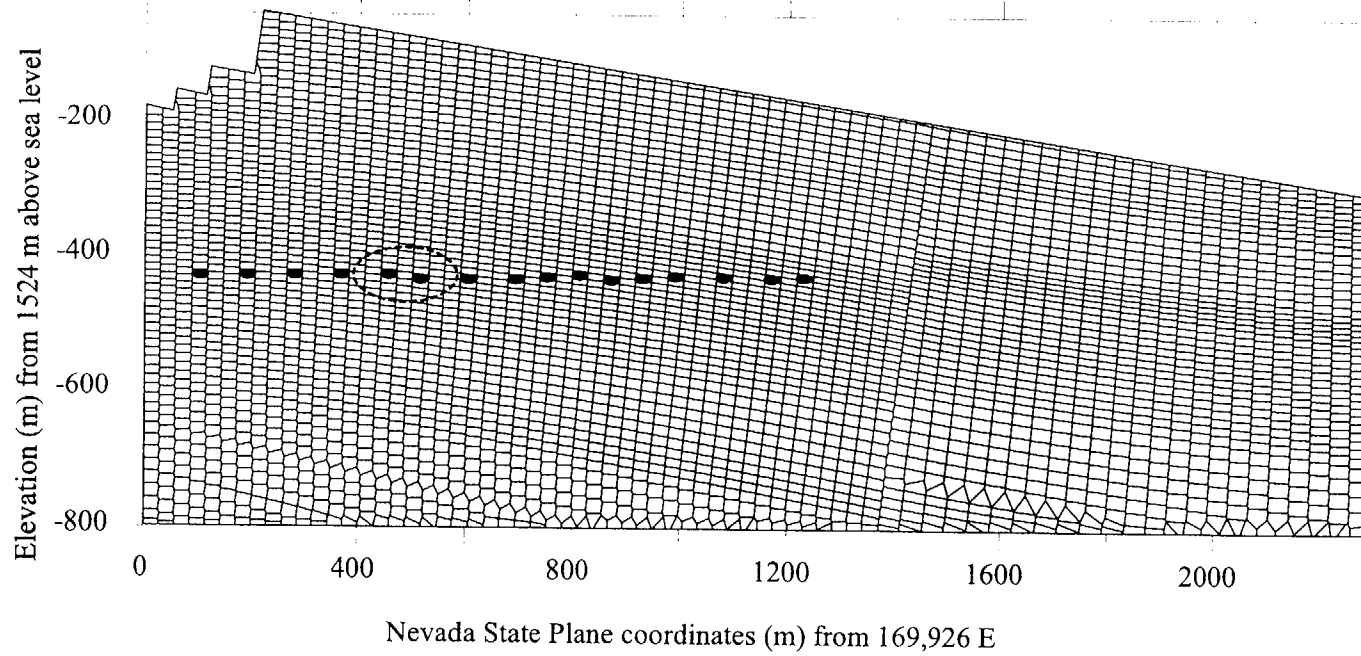


Figure 4-1. Finite difference discretization of an east-west vertical section through Yucca Mountain for TH analyses (from Ofoegbu et al., 2000). Cells used for heat-source application are marked with dark dots. The horizontal ellipse with dashed boundary [centered at (500, -434)] represents a generic TM-altered zone.

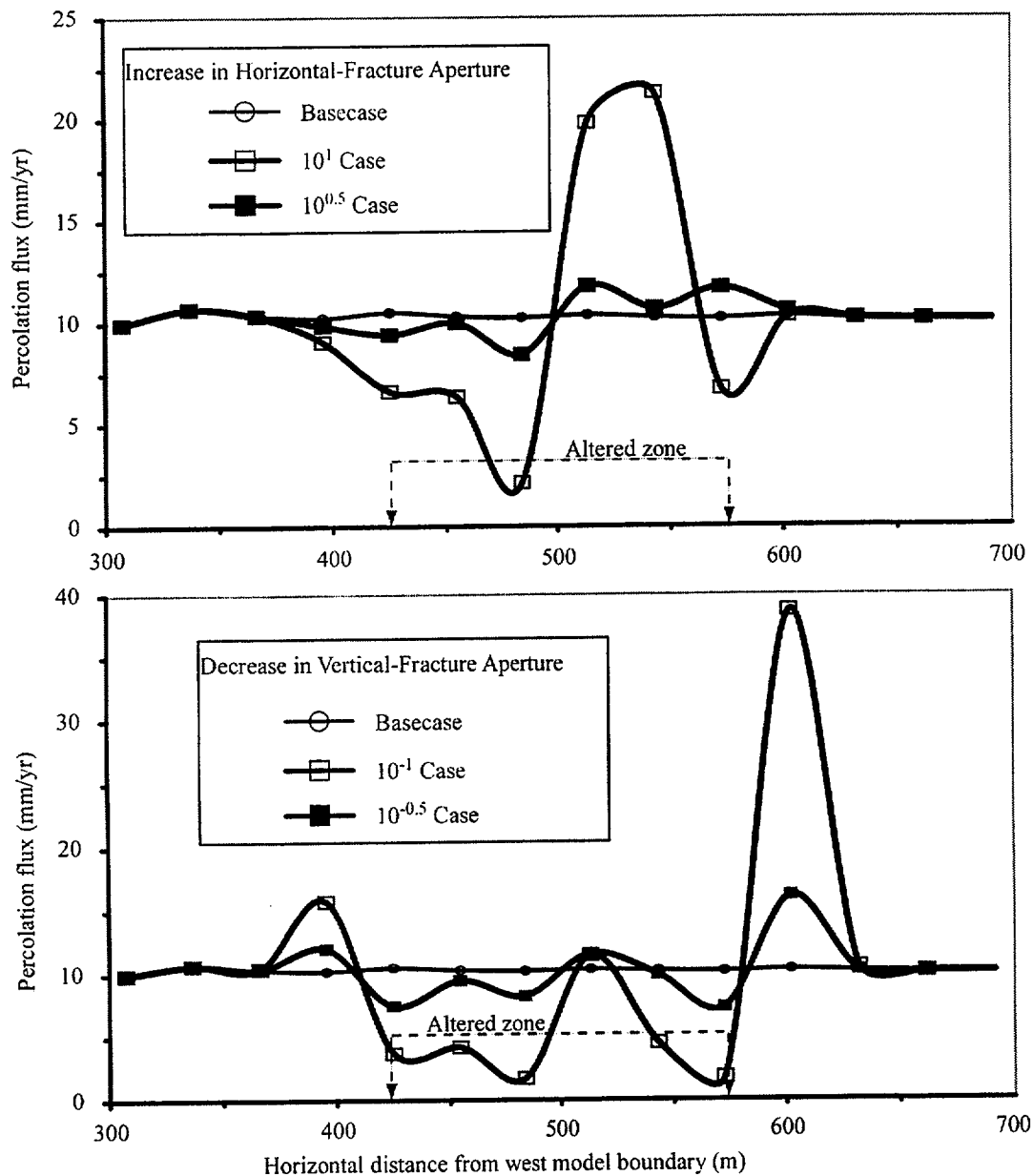


Figure 4-2. Profiles of percolation flux at the repository depth, illustrating the effects of a generic TM-altered zone (from Ofoegbu et al., 2000). Results represent the effects of horizontal-fracture dilation with no change in vertical fractures and vertical-fracture closure with no change in horizontal fractures. Each analysis case is identified using the applied R_b value. Both cases are compared with the basecase in which $R_b=1$ for both horizontal and vertical fractures.

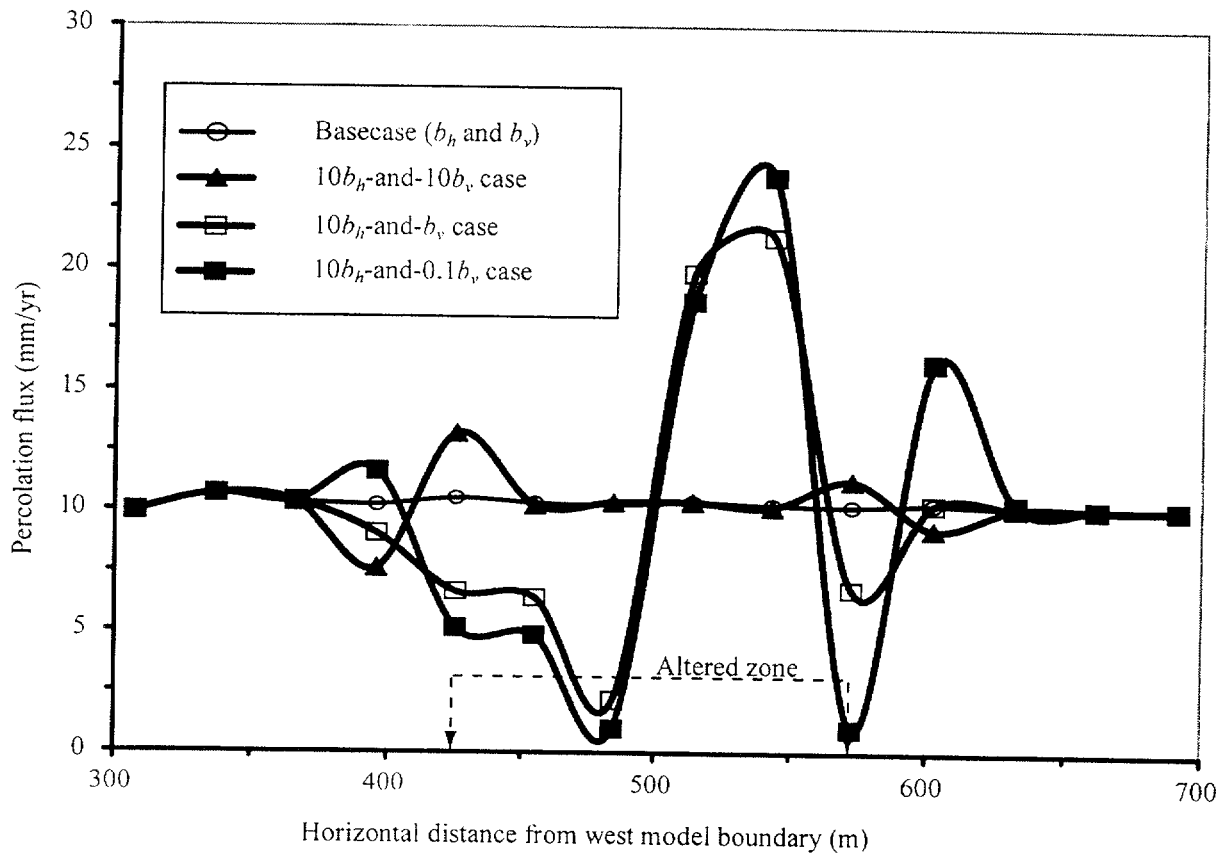


Figure 4-3. Profiles of percolation flux at the repository depth, illustrating the effects of a generic TM-altered zone (from Ofoegbu et al., 2000). Results represent the effects of combining horizontal-fracture dilation with different magnitudes of net vertical-fracture dilation and closure. Parameters b_h and b_v represent the horizontal and vertical fracture apertures for the basecase.

If horizontal-fracture dilation and net vertical-fracture closure occur simultaneously, the effects of horizontal-fracture dilation on flow would be dominant. For example, the $10b_h$ -and- b_v case (representing horizontal-fracture dilation with no change in vertical fractures) and the $10b_h$ -and- $0.1b_v$ case (representing horizontal-fracture dilation with vertical-fracture closure) gave essentially identical results (figure 4-3). Both cases resulted in elevated vertical flux within and on the downstream side of the altered zone, indicating that the effect of horizontal-fracture dilation would be dominant irrespective of the magnitude of simultaneous vertical-fracture closure within a closure ratio of $0.1 \leq R_{bv} \leq 1.0$. The anticipated closure ratio for vertical fractures should fall within this range and would be much closer to 1.0 than 0.1 considering the discussion in section 3.2. Therefore, the anticipated vertical-fracture closure would have less effect on moisture flow than shown in figures 4-2 and 4-3. A simultaneous dilation of horizontal and vertical fractures (e.g., $10b_h$ -and- $10b_v$ case in figure 4-3) may not have as much effect on moisture flux as a combination of horizontal-fracture dilation with the vertical fractures remaining essentially unchanged.

These results show that magnitudes of fracture dilation within a range of $1 \leq R_b \leq 10$ can produce significant effects on repository-level percolation flux, whereas the anticipated magnitudes of fracture closure would not produce any appreciable effect on percolation flux. The models indicate elevated vertical flux within and on the downstream side of the altered zone with a flux magnification factor of up to 4.0, but the value of this factor depends on the magnitudes and orientation of fracture dilation and possibly on the geometry of the altered zone and the infiltration rate. The simulation of a generic TM-altered zone did not include the effects of fracture closure or opening on fracture capillarity. A parallel study is being undertaken to characterize such effects and how they might alter fracture conductivity.¹

¹Personal communication with R. Fedors (May 2000).

5 CONCLUSIONS

Numerical-modeling results are presented in this report to examine (i) changes in rock-mass hydrological properties associated with the anticipated geomechanical response to thermal loading at the proposed YM repository and (ii) the effects of such changes on deep percolation. Changes in hydrological properties are important because of potential effects on the percolation flux through the repository horizon. The percolation flux has significant effects on the (i) occurrence and magnitude of water influx into the emplacement drifts, (ii) onset and rates of WP corrosion, (iii) mobilization of waste into aqueous states, and (iv) transport of radionuclides to the saturated zone.

Information presented in this report will help evaluate the technical bases for (i) a subissue of the Repository Design and Thermal-Mechanical Effects (RDTME) Key Technical Issue (KTI) that addresses DOE estimates of changes in hydrological properties due to thermally induced ground movements, considering the potential effects of such changes on repository performance and (ii) a subissue of the Thermal Effects on Flow (TEF) KTI that addresses the sufficiency of the DOE TH modeling approach to predict the nature and bounds of TEF considering the effects of coupled processes, among other things. DOE has attempted to address these TEF and RDTME subissues by stating that “simulation results indicate that thermal loading will produce negligible changes in rock hydrologic properties.”¹

The following conclusions are presented:

- Rock-mass permeabilities near the repository horizon can be expected to increase within laterally discontinuous zones (referred to as TM-altered zones) centered at the emplacement drifts and in the middle of interdrift pillars, owing to fracture dilation associated with geomechanical response to repository thermal loading.
- The magnitude of permeability increase in the TM-altered zones would be greater around the drift openings than in the pillars, and would depend on thermal loading, rock-mass mechanical properties, and time-dependent mechanical degradation. Analyses presented in this report indicate permeability increases of more than three orders of magnitude near the drifts and up to two orders of magnitude in the pillars.
- The TM-altered zones would be characterized by horizontal-fracture dilation in areas of high rock-mass quality and vertical-fracture dilation in areas of low rock-mass quality. Fracture closure from thermally induced stresses is not expected to produce significant effects on rock-mass permeability.
- Lateral flow of moisture can be expected in the TM-altered zones and would result in the redistribution of percolation flux near the repository horizon. As a result, elevated vertical flux can be expected at the downstream end and within the perimeters of a TM-altered zone. Therefore, parts of an emplacement drift close to the downstream end of a TM-altered zone can be expected to experience elevated percolation flux.

¹Barr, D. Thermal Effects on Flow. *Presentation at DOE/NRC Technical Exchange on Yucca Mountain Pre-Licensing Issues*. Las Vegas, NV: U.S. Department of Energy, Yucca Mountain Site Characterization Office. April 2000.

- Predictions of the geometry of TM-altered zones and associated hydrological-property changes would be affected by the TM characteristics of the rock mass, specifically heat capacity, thermal expansivity, elastic stiffness (Young's modulus), strength parameters (friction angle and cohesion), and time-dependent mechanical degradation. Therefore, the description of these rock-mass characteristics for TM modeling deserves special attention in the review of DOE predictions of TM effects on hydrological properties.
- These findings contrast with a DOE position that "thermal loading will produce negligible changes in rock hydrologic properties,"² which is apparently based on an incorrect upperbound for thermally induced permeability change that was determined from a previous DOE analysis [Blair (in Hardin, 1998)].

²Barr, D. Thermal Effects on Flow. *Presentation at DOE/NRC Technical Exchange on Yucca Mountain Pre-Licensing Issues*. Las Vegas, NV: U.S. Department of Energy, Yucca Mountain Site Characterization Office. April 2000.

6 REFERENCES

- Ahola, M.P., R. Chen, H. Karimi, S.M. Hsiung, and A. Chowdhury. *A Parametric Study of Drift Stability in Jointed Rock Mass. Phase I: Discrete Element Thermal-Mechanical Analysis of Unbackfilled Drifts*. CNWRA 96-009. San Antonio, TX: Center for Nuclear Waste Regulatory Analyses. 1996.
- Bagtzoglou, A.C., N.M. Coleman, E.C. Percy, S.A. Stothoff, and G.W. Wittmeyer. *Unsaturated and Saturated Flow Under Isothermal Conditions*. B. Sagar, ed. NUREG/CR-6513. Washington, DC: Nuclear Regulatory Commission. 1996.
- Bandis, S.C. *Mechanical Properties of Rock Joints*. N.R. Barton and O.V. Stephansson, eds. Rotterdam, Netherlands: A.A. Balkema. 1990.
- Bandis, S.C., A.C. Lumsden, and N.R. Barton. Fundamentals of rock joint deformation. *International Journal of Rock Mechanics and Mining Sciences and Geomechanics Abstracts* 20(6): 249–268. 1983.
- Barton, N., R. Lien, and J. Lunde. Engineering classification of rock masses for the design of tunnel support. *Rock Mechanics* 6: 189–236. 1974.
- Barton, N., S. Bandis, and K. Bakhtar. Strength, deformation, and conductivity coupling of rock joints. *International Journal of Rock Mechanics and Mining Sciences and Geomechanics Abstracts* 22(3): 121–140. 1985.
- Berge, P.A., H.F. Wang, and S.C. Blair. *Estimated Bounds on Rock Permeability Changes from THM Processes*. UCRL-ID-131492. Livermore, CA.: Lawrence Livermore National Laboratory. 1998.
- Berge, P.A., S.C. Blair, and H.F. Wang. Thermomechanical effects on permeability for a 3D model of YM rock. *Rock Mechanics for Industry. Proceedings of the 37th U.S. Rock Mechanics Symposium 2*. B. Amadei, R.L. Kranz, G.A. Scott, and P.H. Smeallie, eds. Rotterdam, Netherlands: A.A. Balkema. 729–734. 1999.
- Brechtel, C.E., M. Lin, E. Martin, and D.S. Kessel. *Geotechnical Characterization of the North Ramp of the Exploratory Studies Facility*. Volume 1—Data Summary. SAND95-0488/1. Albuquerque, NM: Sandia National Laboratories. 1995.
- Carlos, B.A., S.J. Chipera, and D.L. Bish. *Distribution and Chemistry of Fracture-Lining Minerals at Yucca Mountain, Nevada*. LA-12977-MS, UC-814. Los Alamos, NM: Los Alamos National Laboratory. 1995.
- Chen, R. Analyses of drift stability and rockfall due to earthquake ground motion at Yucca Mountain, Nevada. *Rock Mechanics for Industry. Proceedings of the 37th U.S. Rock Mechanics Symposium 2*. B. Amadei, R.L. Kranz, G.A. Scott, and P.H. Smeallie, eds. Rotterdam, Netherlands: A.A. Balkema. 759–766. 1999.

- Chen, R., G.I. Ofoegbu, and S. Hsiung. Modeling drift stability in fracture rock mass at Yucca Mountain, Nevada—Discontinuum approach. *Proceedings of the 4th North American Rock Mechanics Symposium, Seattle, Washington, July 30–August 2000*. Rotterdam, Netherlands: A.A. Balkema. To be published July 2000.
- Civilian Radioactive Waste Management System Management and Operating Contractor. *Repository Thermal Loading Management Analysis*. B00000000–01717–0200–00135. Revision 00. Las Vegas, NV: Civilian Radioactive Waste Management System Management and Operating Contractor. 1997a.
- Civilian Radioactive Waste Management System Management and Operating Contractor. *Confirmation of Empirical Design Methodologies*. BABEE0000–01717–5705–00002. Revision 00. Las Vegas, NV: Civilian Radioactive Waste Management System Management and Operating Contractor. 1997b.
- Civilian Radioactive Waste Management System Management and Operating Contractor. *Repository Ground Support Analysis for Viability Assessment*. BCAA00000–01717–0200–00004. Revision 01. Las Vegas, NV: Civilian Radioactive Waste Management System Management and Operating Contractor. 1998.
- Daily, W., W. Lin, and T. Buscheck. Hydrological properties of Topopah Spring tuff: Laboratory measurements. *Journal of Geophysical Research* 92(B8): 7,854–7,864. 1987.
- Elsworth, D., and C.R. Mase. Chapter 8: Groundwater in rock engineering. *Comprehensive Rock Engineering* 1. J.A. Hudson, ed. New York, Pergamon Press. 201–226. 1993.
- Flint, A.L., J.A. Hevesi, and L.E. Flint. *Conceptual and Numerical Model of Infiltration for Yucca Mountain Area, Nevada*. U.S. Geological Survey Water Resources Investigations Report. 1996.
- Geomatrix Consultants, Inc. *Near-Field/Altered Zone Coupled Effects Expert Elicitation Project*. Las Vegas, Nevada: Geomatrix Consultants, Inc. 1998.
- Hardin, E.L. *Near-Field/Altered-Zone Models Report*. UCRL–ID–129179. Livermore, CA: Lawrence Livermore National Laboratory. 1998.
- Hevesi, J.A., and A.L. Flint. *Geostatistical Model for Estimating Precipitation and Recharge in the Yucca Mountain Region, Nevada–California*. U.S. Geological Survey Water Resources Investigations Report 96-4123. 1996.
- Hibbit, Karlsson & Sorensen, Inc. *ABAQUS Users' Manual Version 5.8*. Pawtucket, RI: Hibbit, Karlsson & Sorensen, Inc. 1998.
- Hoek, E., and E.T. Brown. Practical estimates of rock mass strength. *International Journal of Rock Mechanics and Mining Sciences and Geomechanics Abstracts* 34(8): 1,165–1,186. 1997.
- Hsiung, S.M., D.D. Kana, M.P. Ahola, A.H. Chowdhury, and A. Ghosh. *Laboratory Characterization of Rock Joints*. NUREG/CR–6178. Washington, DC: Nuclear Regulatory Commission. 1994.

- Jaeger, J.C., and N.G.W. Cook. *Fundamentals of Rock Mechanics*. 3rd Edition. London: Chapman and Hall. 1979.
- Kenney, T.C. The influence of mineralogical composition on the residual strength of natural soils. *Proceedings of the Oslo Geotechnical Conference on the Shear Strength Properties of Natural Soils and Rocks, I*: Norwegian Geotechnical Institute. Oslo, Norway. 123–129. 1967.
- Lajtai, E.Z., and R.H. Schmidtke. Delayed failure in rock loaded in uniaxial compression. *Rock Mechanics and Rock Engineering* 19: 11–25. 1986.
- Levy, S.S., D.T. Vaniman, D.L. Bish, G. WoldeGabriel, S.J. Chipera, J.W. Carey, P. Dixon, S.J. Goldstein, and M.T. Murrell. *Summary and Synthesis Report on Mineralogy and Petrology Studies for the Yucca Mountain Site Characterization Project, Volume II: History of Mineralogic and Geochemical Alteration of Yucca Mountain*. Los Alamos, NM: Los Alamos National Laboratory. 1996
- Lichtner, P.C., G. Keating, and B. Carey. *A Natural Analogue for Thermal-Hydrological-Chemical Coupled Processes at the Proposed Nuclear Waste Repository at Yucca Mountain, Nevada*. LA-13610-MS. Los Alamos, NM: Los Alamos National Laboratory. 1999.
- Lichtner, P.C., M.S. Seth, and S. Painter. *MULTIFLO User's Manual, MULTIFLO Version 1.2: Two-Phase Nonisothermal Coupled Thermal-Hydrological-Chemical Flow Simulator*. San Antonio, TX: Center for Nuclear Waste Regulatory Analyses. 2000.
- Lin, W., and W. Daily. *Transport Properties of Topopah Spring Tuff*. UCRL-53602. Livermore, CA: Lawrence Livermore National Laboratory. 1984.
- Matyskiela, W. Silica redistribution and hydrologic changes in heated fractured tuff. *Geology* 25(12): 1,115–1,118. 1997.
- Mitchell, J.K. *Fundamentals of Soil Behavior*. New York: John Wiley and Sons, Inc. 1976.
- Murphy, W.M. Geochemical Models for Gas-Water-Rock Interactions in a Proposed Nuclear Waste Repository at Yucca Mountain, Nevada. *Proceedings of the Topical Meeting on Site Characterization and Model Validation, Focus '93, Las Vegas, Nevada, September 26–29, 1993*. La Grange Park, IL: American Nuclear Society: 115–121. 1993.
- Nuclear Regulatory Commission. *Issue Resolution Status Report, Key Technical Issue: Repository Design and Thermal-Mechanical Effects*. Revision 2. Washington, DC: Nuclear Regulatory Commission. 1999.
- Ofoegbu, G.I. Variations of drift stability at the proposed Yucca Mountain repository. *Rock Mechanics for Industry. Proceedings of the 37th U.S. Rock Mechanics Symposium 2*. B. Amadei, R.L. Kranz, G.A. Scott, and P.H. Smeallie, eds. Rotterdam, Netherlands: A.A. Balkema. 767–773. 1999.
- Ofoegbu, G.I., and J.H. Curran. Deformability of intact rock. *International Journal of Rock Mechanics and Mining Sciences and Geomechanics Abstracts* 29(1): 35–48. 1992.

- Ofoegbu, G.I., and D.A. Ferrill. *Finite Element Modeling of Listric Normal Faulting*. CNWRA 95-008. San Antonio, TX: Center for Nuclear Waste Regulatory Analyses. 1995.
- Ofoegbu, G.I., S. Painter, R. Chen, R.W. Fedors, and D.A. Ferrill. Geomechanical and thermal effects on moisture flow at the proposed Yucca Mountain nuclear waste repository. *Nuclear Technology*. 2000. In Review.
- Snow, D.T. Rock fracture spacings, openings, and porosities. Proceedings of the American Society of Civil Engineers. *Journal of the Soil Mechanics and Foundations Division* 94(SM1): 73–91. 1968.
- Stothoff, S.A. Sensitivity of long-term bare soil infiltration simulations to hydraulic properties in an arid environment. *Water Resources Research* 33(4): 547–558. 1997.
- Thoma, S.G., D.P. Gallegos, and D.M. Smith. Impact of fracture coatings on fracture/matrix flow interactions in unsaturated, porous media. *Water Resources Research* 28(5): 1,357–1,367. 1992.
- TRW Environmental Safety Systems, Inc. *License Application Design Selection Report*. B00000000–01717–4600–00123. Revision 01. Las Vegas, NV: TRW Environmental Safety Systems, Inc. 1999.
- U.S. Department of Energy. *Repository Safety Strategy: U.S. Department of Energy's Strategy to Protect Public Health and Safety After Closure of a Yucca Mountain Repository*. YMP/96–01. Revision 01. Washington, DC: U.S. Department of Energy. 1998a
- U.S. Department of Energy. *Viability Assessment of a Repository at Yucca Mountain. Volume 1: Introduction and Site Characteristics*. DOE/RW–0508/V1. Las Vegas, NV: U.S. Department of Energy, Office of Civilian Radioactive Waste Management. 1998b.
- U.S. Department of Energy. *Viability Assessment of a Repository at Yucca Mountain. Volume 2: Preliminary Design Concept for the Repository and Waste Package*. DOE/RW–0508/V2. Las Vegas, NV: U.S. Department of Energy, Office of Civilian Radioactive Waste Management. 1998c.
- Wei, Z.Q., P. Egger, and F. Descoeurdes. Permeability predictions for jointed rock masses. *International Journal of Rock Mechanics and Mining Sciences and Geomechanics Abstracts* 32(3): 251–261. 1995.

